EURASIAN JOURNAL OF MATHEMATICAL AND COMPUTER APPLICATIONS
ISSN 2306–6172
Volume 3, Issue 4 (2015) 4-44

MATHEMATICAL MODELS AND ALGORITHMS FOR RECONSTRUCTION OF SINGULAR SUPPORT OF FUNCTIONS AND VECTOR FIELDS BY TOMOGRAPHIC DATA

E.Yu. Derevtsov, S.V. Maltseva, I.E. Svetov

Abstract A problem of reconstruction of singularities of given in a unit disk scalar and vector fields is investigated. The Radon and ray transforms serves as initial date for the problem. Tools of mathematical modeling and numerical experiments are applied. Specially the task of visualization of lines of the fields and their derivatives breaks is considered. We propose the operators of indicators of inhomogeneity and breaks for the numerical solution to the problem. This indicators are constructed on a base of the differential operators and the integral operators of back-projection and angular moments. Suggested approaches serve as a basis for the algorithms which are realized numerically and investigated by simulation tests.

Key words: tomography, Radon transform, ray transform, vector field, non-smooth function, singular support, back-projection operator, tensor analysis

AMS Mathematics Subject Classification: 44A12, 65R10, 65R32

Introduction

A rapid development of tomographic methods in science investigations and medical diagnostic, which began in the second half of XX century, was due to two significant achievements. At first it is the invention of methods of the signal detection allowing to assume that signal propagates along the line. Secondly, it is the extension of fast-acting computers, which enable to process large amounts of data. Development and extension of applications of tomography continues nowadays and captures new areas of human activity.

Mathematical foundations of tomography were laid in the articles [1], [2], where inversion formulas for the problem of integral geometry, posed on the plane, in the space, and on the sphere $\mathbb{S}^2$ were obtained. The idea of these formulas was to specify the sequence of actions in order to find unknown function given on the plane, in the space or on the unit sphere by known integrals calculated over all straight lines (on the plane); over all planes (in $\mathbb{R}^3$); along all big circles of the sphere $\mathbb{S}^2$, respectively.

Let's emphasize main features and characteristics of tomographic methods. The distinctive and attractive feature of these investigations is that measuring methods do not destroy the object. In the vast majority of mathematical models in tomography the ray approximation is used. Information about the medium is "accumulated" along the ray and is registered at the output. The inalienable feature of tomography is multiple measurements of the same type, which allows to obtain the enough data capacity. By

virtue of incorrectness of the tomography problem the insufficiency of the data leads to the great arbitrariness in the solution, and the measurement uncertainties lead to its instability.

The significant extension of application areas and statements of the tomography problems have led to the appearance of its varieties such as vector, tensor, refraction one. The becoming and the rapid development of the listed divisions of tomography is largely based on the ideas, statements and results of integral geometry developed in the framework of more general theory of inverse and ill-posed problems. The term "integral geometry" means certain class of inverse problems, closely connected with geometrical objects in the space of arbitrary dimension, see for example [3], [4], [5], [6], [7], [8], [9], [10], [11], [12]. A powerful incentive for the development of statements of integral geometry was geophysical investigations, [13]. With a formation of tomography as independent natural science and practical discipline the statements and results of integral geometry turned out to be claimed in many areas connected with researches by nondestructive methods.

A large variety of algorithms are used for solving tomography problems. We shall mention main mathematical tools on which they are founded. Above all we note inversion formulas which are a basis of a family of algorithms known as algorithms of convolution and back-projection, [14], [15], [16]. A development of the mentioned approach led to the algorithms of Davison-Grunbaum, Masih-Nelson, ρ-filtration back-projection, Marr and others, [17]. Secondly, the other class of algorithms is based on the projection theorems, [18], [19]. Thirdly, algebraic methods, see [20], [21], got wide expansion.

Most part of algorithms may be applied not only to the problems of scalar but also to the problems of vector and tensor tomography. However, a few exceptions, almost all of them may be applied only in the frameworks of mathematical models for mediums without refraction. But if the refraction phenomenon is included in a mathematical model of the medium then the list of useful mathematical instruments becomes poor. We note two of these methods. The first one is the least square method which may be applied for solving problems where initial data are the integrals along curves, and in particular along geodesics of Riemannian metric. The second one is a method of singular value decomposition.

A problem of breaks reconstruction. There are a lot of practically important natural and technical areas with investigated objects mathematically described by breaking values. The objects of such kind arise in tomographic problems often. Thus, a detection of cracks in manufactured products by nondestructive control is no less important task then a reconstruction of its internal structure. In many geophysical problems determination of boundaries locations, which separates blocks with different physical properties, often is the first stage for further researches.

An exact description of objects with breaks in the frameworks of integral geometry was proposed in the monograph [4], and then, for example, in articles [22], [23]. An application of numerical methods and algorithms developed for the reconstruction of smooth (at least differentiable) functions gives an unsatisfactory results in a case of discontinuous functions. One way for reconstruction of this function is to apply well-known in tomography algorithmic tools, but it is necessary extremely to increase the

amount of initial data and the calculation accuracy. The second way is to develop special algorithmic tools for reconstruction of such functions. It is possible to describe the posed problem by listing the stages of its solving: a) a visualization of a set of break points of a function under investigation; b) a localization of this set and its approximate description in frameworks of discrete model of the investigated object; c) a determination (by the set of break points was found on previous steps) of values of the jump characterizing the break; d) an elimination of breaks and reconstruction of the auxiliary function without breaks; e) a reconstruction of the initial discontinuous function with usage of the previously found jump values.

A term "visualization of breaks" means an obtaining the picture with well-recognized set of break points of the function. It may be sharp boundary in color or gray-scale images, or sharp increase of function near break points if the image is presented by relief. Under localization of a set of break points we assume its rigorous description in mathematical terms. For example, approximate determination of coordinates of break points and assignment (by equations) of the approximation of lines or surfaces consisting of break points.

The problem of determination of the jump value at the break point is clear and does not require additional clarification. Items d) and e) are closely connected. In essence it requires to construct the function eliminating breaks and to use it twice. It should be noted that in overwhelming majority of articles the item a) is meant as the problem of breaks reconstruction. This qualitative information is often enough in many practical tasks. In several articles the problem of determination the jump values is considered.

The first approach to the visualization of a set of break points of a function by its Radon transform was proposed in [24]. Its sense consists in double differentiation with respect to s ($|s|$ is a distance from the origin to the line along which the integration is held) of the Radon transform followed by usage of the back-projection operator. This sequence of actions was named *Vainberg operator*. The application of the operator does not give the sought-for function, in opposite with inversion formulas, but leads to the visualization of the set of break points. In [5] following justification of application of the Vainberg operator was proposed. Namely, this operator reconstructs a function $(-\Delta)^{1/2} f$ (Δ is Laplace operator). Since $(-\Delta)^{1/2}$ is elliptic pseudo-differential operator, then function $(-\Delta)^{1/2} f$ has the same singularities as f. This idea may be designed for inversion the Radon transform $\mathcal{R}f$ of non-smooth function f. We have to check only that the Radon transform of the Laplace operator Δ (on functions $f(x, y)$) turns into the operator $\partial^2/\partial s^2$ (on functions $(\mathcal{R}f)(\alpha, s)$). Thus if we have now a distribution f, presented in the form $f = (1 - \Delta)^k p$ (where p has necessary smoothness, k is natural), then we can determine the Radon transform of function f as a convolution $F((1 + s^2)^k) * (\mathcal{R}p)$. After calculating the convolution $\mathcal{R}f$ with $(1 + s^2)^{-k}$ we obtain sufficiently smooth function $\mathcal{R}p$. By means of an inversion formula for the Radon transform we find function p and then, applying to the last one the differential operator $(1 - \Delta)^k$, we obtain sought-for function f.

Further development of methods and algorithms for reconstruction of the set of break points was suggested, for example in [25], [26], [27], [28]. In the papers the inversion operator $(-\Delta)^{1/2}$ in combination with regularization or certain filtration was used alongside with the Vainberg operator. The main goal of researches was to reconstruct

the set of break points as well as to determine some average characteristics of smooth part of the object.

At the end of 90-th years one more approach to the solution of the problem of determination of the set of functions breaks by the Radon transform was proposed. The approach is based on the theory of multidimensional singular integrals [29]. After an application of the back-projection operator to the Radon transform and then a differentiation with respect to spacial variables leads to logarithmic increase of the result as the point tends to a break line. In particular, the operator $|\nabla(\cdot)|$ may be used, [30], [31], [23].

A reconstruction of singular support. Recent years due to intensive progress of vector and tensor tomography the statement of the problem of breaks reconstruction was significantly generalized (see for example [32], [33]), and nowadays it may be interpreted as the problem of reconstruction of singular support of symmetric tensor fields by their known ray transforms. The singular support means a set of points of a field in which a condition of its infinite smoothness is broken. Consequently, the problem of breaks reconstruction is posed not only for the fields but also for their derivatives. A generalization of the problem of reconstruction of breaks for function leads to the necessity of development suitable methods and algorithms for reconstruction of the set of points of singular support of tensor fields by their ray transforms, or more widely, by tomographic data.

As for the problem of reconstruction of discontinuous functions there exist several ways for the reconstruction of the singular support of tensor fields by their known ray transforms. The first is to apply well-known in tomography algorithmic tools, taking into account its modification, for the reconstruction of vector or tensor fields, probably given in media with refraction. Numerical tests show that the recovering accuracy of non-smooth objects, in comparison with continuous, is in 5–10 times worse. As for the problem of reconstruction of discontinuous functions, it is necessary to have sharply increasing amount of initial tomographic data and therefore increase of time of computations for achievement of acceptable accuracy of results. The second way is to design special algorithmic tools for the reconstruction of the singular support of a tensor field. The approach is similar to the approach for the discontinuous functions. It is described in details at items a)–e) above.

There is the third way for reconstruction of vector and tensor fields with nonempty singular support. The way cannot be applied to the problem of reconstruction of singular support of a function. Namely, we say about the reconstruction of potentials of fields. It is known that the smoothness of potentials is more than the smoothness of the fields themselves. As the potentials are at least continuous, an accuracy of their reconstruction by usual tools is in 5-10 times better then the accuracy of reconstruction of the fields, generated by these potentials. Let's note that the problem of visualization of a set of points of singular support of a tensor field is correct. It is clear from the statement in which nonlocal pseudo-differential operator is replaced by the local differential one. Mathematical description of the set of singular support requires to use approaches essentially differing from others usually used in tomography. This is due to the considered problem inherently refers to the problem of pattern recognition and latter of data approximation. Probably the problem concerns such mathematical

subjects as statistic data analysis, description of classes of objects, etc.

We represent short content of the article. Introduction contains main theses, features and facilities of tomography. We pay attention on main mathematical approaches and developed in framework of tomographic statements numerical methods and algorithms. The problem of reconstruction of discontinuous functions, and then a single support of functions and vector fields is discussed in more details. In section 1 we represent preliminary tools such as main operators and transforms of tensor tomography. Section 2 contains the ways of the operators of breaks indicators construction for the functions and vector fields. The algorithms for breaks reconstruction of functions, vector fields and their derivatives as well as the results of numerical simulations are sated in section 3. Section 4 is devoted to the numerical results of reconstruction of singular support of functions and vector fields. Conclusion contains a summary, some questions and directions of further investigations.

The article presents a review based in the main on the results of the authors published partially at [33], [34], [35], [36], [37].

1 Preliminary definitions and results

Let's introduce following designations: $B = \{(x^1, x^2) \in \mathbb{R}^2 \,|\, (x^1)^2 + (x^2)^2 < 1\}$ is a unit disk with center in the origin; $\partial B = \{(x^1, x^2) \in \mathbb{R}^2 \,|\, (x^1)^2 + (x^2)^2 = 1\}$ is a unit circle; $Z = \{(\alpha, s) \in \mathbb{R}^2 : \alpha \in [0, 2\pi], s \in [-1, 1]\}$ is a cylinder $[-1, 1] \times [0, 2\pi]$. Unit vectors $\xi \in \partial B, \xi = (\cos\alpha, \sin\alpha)$, $\eta := \xi^\perp \in \partial B$, $\eta = (-\sin\alpha, \cos\alpha)$ and a real number $s \in \mathbb{R}$ specify a line $L_{\xi,s}$ in the form of normal equation $x^1\cos\alpha + x^2\sin\alpha - s = 0$, or parametric equations $x^1 = s\cos\alpha - t\sin\alpha,\ x^2 = s\sin\alpha + t\cos\alpha$.

We denote functions (scalar fields) as $f(x), g(x), \ldots$. For potentials specifying tensor fields we use designations $\varphi(x), \psi(x), \chi(x), \ldots$. It is assumed that they are given in $B \subset \mathbb{R}^2$. Designations $x = (x^1, x^2)$, $y = (y^1, y^2), \ldots$ are convenient for the statement of the problems and formulations of properties of tensor fields, but sometimes, especially at description of numerical tests, we use designations (x, y) also. A set of given in B symmetric m-tensor fields $w(x) = (w_{i_1\ldots i_m}(x))$, $u(x) = (u_{i_1\ldots i_m}(x))$, $v(x) = (v_{i_1\ldots i_m}(x))$, $\ldots$, $i_1, \ldots, i_m = 1, 2$, has a designation $S^m(B)$. Scalar product in $S^m(B)$ is established by the formula

$$\langle u(x), v(x)\rangle = u_{i_1\ldots i_m}(x)v^{i_1\ldots i_m}(x),$$

where the summation over repeating top and bottom eponymous indexes from 1 to 2 is meant. We use the covariant components of tensor fields below.

We would like to remind the notations for functional spaces. There are the spaces of functions integrable with square $L_2(B)$, symmetric m-tensor fields $L_2(S^m(B))$, L_2-space $L_2(Z)$. Symmetric m-tensor fields u, v are elements of $L_2(S^m(B))$ with scalar product

$$(u, v)_{L_2(S^m(B))} = \int_B \langle u(x), v(x)\rangle dx.$$

Spaces of differentiable (with the finite order k) symmetric m-tensor fields are denoted as $C^k(S^m(B))$, $C_0^k(S^m(B))$. Sobolev spaces are denoted as $H^k(S^m(B))$, $H_0^k(S^m(B))$, $H^k(Z)$, and are defined as usual, $m = 0, 1, 2, \ldots$; $k = 0, 1, \ldots$. Somewhere below we use the spaces of basic functions $\mathcal{D}(B)$, $\mathcal{D}(\mathbb{R}^2)$, and Schwartz spaces $\mathcal{S}$, $\mathcal{S}'$.

We consider following classes of discontinuous functions, vector and tensor fields. Let a domain $D \subset R^2$ (probably multiply connected) be such that $\overline{D} \subset B$ consists of finite number of nonoverlapping subdomains $\{D_i\}$, $i = 1, \ldots, N$, with the dense in $\overline{D}$ union $D_0 = \cup D_i$. The boundaries belong to C^1-class of smoothness. It is easy to see that $\partial D \subset \partial D_0$ and the boundary ∂D_0 coincides with the union of boundaries $\cup D_i$ of subdomains D_i, $i = 1, \ldots, N$. Three classes of functions in $\overline{D} \subset B$ are considered. The first one is $\mathcal{C}^{-1}(B)$. It contains functions with breaks at the points $(x, y) \in \partial D_0$. The first class serves for description of discontinuous scalar fields. The second class $\mathcal{C}^0(B)$ consists of continuous functions with discontinuous first derivatives at the points belonging the set $(x, y) \in \partial D_0$. This class of functions are the potentials for discontinuous vector fields. Finally, the third class $\mathcal{C}^1(B)$ consists of the functions with continuous derivatives and discontinuous second derivatives at the points $(x, y) \in \partial D_0$. The functions are the potentials for discontinuous symmetric 2-tensor fields. All breaks are assumed to be breaks of the first kind as it is clear from physical considerations. Below we skip the symbol "B" in designations of classes of functions. The potentials $\varphi(x, y)$, $\psi(x, y)$, $\chi(x, y)$, ... from C^k, $k = -1, 0, 1$, are defined in B, vanish at the set $B \setminus \overline{D}$, and their support coincides with closure of D, $\operatorname{supp} \varphi = \overline{D}$. The potentials are infinitely differentiable at the points $(x, y) \in D$. As for the points belonging ∂D_0, so all partial derivatives $\partial^l \varphi / \partial x^j \partial y^{l-j}$, $l = 0, \ldots, k$, $j \le l$, up to the order k, are continuous, but the derivatives of $k + 1$ order have breaks. We say that function φ is *the potential of $\mathcal{C}^k$-smoothness* or *$\mathcal{C}^k$-potential* in R^2. We remind that k takes values from -1 to 1. In general an increase of k leads to increase of smoothness of corresponding scalar, vector and 2-tensor fields.

1.1 The operators of tensor tomography

Operators of inner differentiation d and orthogonal inner differentiation $\mathrm{d}^\perp$ are generalizations of operators of gradient and orthogonal gradient. The operator of inner differentiation $\mathrm{d} : \mathcal{C}^k(S^m) \to \mathcal{C}^{k-1}(S^{m+1})$, $k \ge 0$, acts on symmetric m-tensor field w and gives symmetric $(m + 1)$-tensor field u by the rule

$$u_{i_1 \ldots i_m j} := (\mathrm{d}w)_{i_1 \ldots i_m j} = \frac{1}{m+1} \Big(\frac{\partial w_{i_1 \ldots i_m}}{\partial x^j} + \sum_{k=1}^{m} \frac{\partial w_{i_1 \ldots i_{k-1} j i_{k+1} \ldots i_m}}{\partial x^{i_k}} \Big).$$

The operator $\mathrm{d}^\perp : \mathcal{C}^k(S^m) \to \mathcal{C}^{k-1}(S^{m+1})$, $k \ge 0$, of inner orthogonal differentiation acts by the rule

$$v_{i_1 \ldots i_m j} := (\mathrm{d}^\perp w)_{i_1 \ldots i_m j} = \frac{1}{m+1} \Big((-1)^j \frac{\partial w_{i_1 \ldots i_m}}{\partial x^{3-j}} + \sum_{k=1}^{m} (-1)^{i_k} \frac{\partial w_{i_1 \ldots i_{k-1} j i_{k+1} \ldots i_m}}{\partial x^{3-i_k}} \Big).$$

Here $w \in \mathcal{C}^k(S^m)$, $u, v \in \mathcal{C}^{k-1}(S^{m+1})$, $k \ge 0$. Operators of divergence δ and orthogonal divergence $\delta^\perp$, δ, $\delta^\perp : \mathcal{C}^k(S^m) \to \mathcal{C}^{k-1}(S^{m-1})$, $k \ge 0$, act on symmetric m-tensor field w,

$$u_{i_1 \ldots i_{m-1}} := (\delta w)_{i_1 \ldots i_{m-1}} = \frac{\partial w_{i_1 \ldots i_{m-1} j}}{\partial x^j} \equiv \frac{\partial w_{i_1 \ldots i_{m-1} 1}}{\partial x^1} + \frac{\partial w_{i_1 \ldots i_{m-1} 2}}{\partial x^2},$$

$$v_{i_1 \ldots i_{m-1}} := (\delta^\perp w)_{i_1 \ldots i_{m-1}} = (-1)^j \frac{\partial w_{i_1 \ldots i_{m-1} j}}{\partial x^{3-j}} \equiv -\frac{\partial w_{i_1 \ldots i_{m-1} 1}}{\partial x^2} + \frac{\partial w_{i_1 \ldots i_{m-1} 2}}{\partial x^1},$$

and give the symmetric tensor fields u, v of $m-1$ rank.

Operators of ray transforms $\mathcal{P}_m^{(j)} : \mathcal{C}^k(S^m) \to \mathcal{C}^k(Z)$, $j = 0, 1, 2$, $k \geq -1$, acting on symmetric tensor field $w = (w_{i_1,\dots i_m})$ and converting them to the functions $g^{(j)}(\xi(\alpha), s)$, defined on the cylinder Z, are specified by the expression

$$\big(\mathcal{P}_m^{(j)} w\big)(\xi, s) = \int_{-\infty}^{\infty} w_{i_1 \dots i_m} \xi^{i_1} \dots \xi^{i_j} \eta^{i_{j+1}} \dots \eta^{i_m} dt, \tag{1}$$

$\xi = (\cos\alpha, \sin\alpha)$, $\eta = (-\sin\alpha, \cos\alpha)$. At $j = 0$ it is longitudinal ray transform $\mathcal{P}$, and integrand includes the components of direction vector (for a line along which integration is hold) η only.

$$\big(\mathcal{P} w\big)(\xi, s) := \big(\mathcal{P}^{(0)} w\big)(\xi, s) = \int_{-\infty}^{\infty} w_{i_1 \dots i_m} \eta^{i_1} \dots \eta^{i_m} dt;$$

At $j = m$ it is transverse ray transform $\mathcal{P}^{\perp}$, and the integrand includes the components of the normal vector ξ only.

$$\big(\mathcal{P}^{\perp} w\big)(\xi, s) := \big(\mathcal{P}^{(m)} w\big)(\xi, s) = \int_{-\infty}^{\infty} w_{i_1 \dots i_m} \xi^{i_1} \dots \xi^{i_m} dt.$$

For one of j, $j = 1, 2, \dots, m-1$, it is mixed ray transform $\mathcal{P}_m^{(j)}$. It includes the components of both normal and direction vectors.

We state formulas for differentiation operators of the image of ray transform (1) with respect to its arguments s and α. As $\big(\mathcal{P}_m^{(j)} w\big)(\alpha, s) \in \mathcal{C}^k(Z)$, $k \geq 0$, is a function depending on s and the angle α, so

$$D_s^{(l)}(\alpha, s) := \frac{\partial^l \big(\mathcal{P}_m^{(j)} w\big)(\alpha, s)}{\partial s^l}, \quad D_\alpha^{(n)}(\alpha, s) := \frac{\partial^l \big(\mathcal{P}_m^{(j)} w\big)(\alpha, s)}{\partial \alpha^n},$$

for $l, n \leq k+1$.

Operator of (n, l)-angular moment maps functions $h(\xi(\alpha), s)$ given on the cylinder Z into symmetric n-tensor fields given in $\mathbb{R}^2$ according to the rule

$$\big(f_n^{(l)}\big)_{i_1 \dots i_n}(x, y) = \frac{1}{2\pi} \int_0^{2\pi} \xi^{i_1} \dots \xi^{i_l} \eta^{i_{l+1}} \dots \eta^{i_n} h\big(\xi(\alpha), s(x, y, \alpha)\big) dt.$$

Here $\xi = \xi(\alpha)$, $\eta = \eta(\alpha)$, $s = s(x, y, \alpha) := x\cos\alpha + y\sin\alpha$. Back-projection operator is a special case of the operator of angular moment. Let the image $g_m^{(j)}(\xi(\alpha), s)$ of the mixed ray transform $\big(\mathcal{P}_m^{(j)} w\big)(\xi, s)$ of symmetric m-tensor field be given. Then back-projection operator $\big(\mathcal{P}\big)^{\#} : C^k(Z) \to \mathcal{S}'(S^m)$ is posed by the equation

$$\big(\mu_m^{(j)}\big)_{i_1 \dots i_m}(x, y) = \frac{1}{2\pi} \int_0^{2\pi} \xi^{i_1} \dots \xi^{i_j} \eta^{i_{j+1}} \dots \eta^{i_m} g_m^{(j)}\big(\xi(\alpha), s(x, y, \alpha)\big) dt,$$

where $\mathcal{S}'(S^m)$ — Schwartz space of slow-growing at infinity symmetric m-tensor fields. In other words, $\big(\mu_m^{(j)}\big)(x, y) = \big(\mathcal{P}^{\#}(\mathcal{P}_m^{(j)} w\big)(x, y)$.

The operators of differentiation $D_s^{(l)}$ and $D_\alpha^{(n)}$, angular moment and back-projection act on images of ray transforms. The listed above operators of tensor analysis d, $\mathrm{d}^\perp$, δ, $\delta^\perp$, act on symmetric tensor fields $\left(f_n^{(l)}\right)_{i_1\dots i_n}(x,y)$ or $\left(\mu_m^{(j)}\right)_{i_1\dots i_m}(x,y)$, which are the results of an application of the operators of angular moment or back-projection.

The Radon transform and its inversion. Let a function $\varphi(x)$, $x=(x^1,x^2)$, be given in B, $\varphi(x)\in\mathcal{C}^k(B)$. The Radon transform $\mathcal{R}\varphi$ of function φ,

$$(\mathcal{R}\varphi)(\xi,s)=\int_{-\infty}^{\infty}\varphi(s\xi+t\xi^\perp)dt \tag{2}$$

are the integrals along straight lines $L_{\xi,s}=\{x\in\mathbb{R}^2 \mid \xi^1x^1+\xi^2x^2=s\}$.

Let $g(\xi,s)\in C^k(Z)$, $g(\xi,s)=(\mathcal{R}\varphi)(\xi,s)$ be the Radon transform for some function $\varphi\in\mathcal{C}^k(B)$. Substituting (2) into the formula

$$f(x)=(\mathcal{R}^\# g)(x)=\frac{1}{2\pi}\int_0^{2\pi}(\mathcal{R}\varphi)(\xi(\alpha),x^1\cos\alpha+x^2\sin\alpha)\,d\alpha,$$

for back-projection operator, we obtain

$$f(x)=\frac{1}{2\pi}\int_0^{2\pi}\left(\int_{-\infty}^{\infty}\varphi(s\xi+t\xi^\perp)\,dt\right)\,d\alpha,$$

and then, after changing variables the representation

$$f(x)=\frac{1}{\pi}\int_{-\infty}^{\infty}\frac{\varphi(y)}{|x-y|}\,dy \tag{3}$$

for $f(x)$ as a convolution, $f=\varphi*|x|^{-1}/\pi$. After application of the Fourier transform to both parts of (3) and using the convolution theorem we come to the expression $F[f]\equiv\widehat{f}$ $=\widehat{\varphi}\cdot h$, where $\widehat{\varphi}\equiv F[\varphi]$, $h=\left(|x|^{-1}\right)\widehat{\ }$, from which $\widehat{\varphi}=\widehat{f}\,/\,h$. The application of the inverse Fourier transform leads to the simple inversion formula

$$\varphi(x)=\frac{1}{2}\int_{-\infty}^{\infty}\frac{\widehat{f}(y)}{h(y)}\,\mathbf{e}^{\mathbf{i}\langle x,y\rangle}\,dy,$$

which is a base of the simple algorithm with a usage of the Fourier transform (direct and inverse).

In the articles of applied nature the following inversion formulas are well known,

$$\varphi(x^1,x^2)=-\frac{1}{4\pi^2}\int_0^{2\pi}\int_{-\infty}^{\infty}\frac{(\mathcal{R}\varphi)'_s(\alpha,s+x^1\cos\alpha+x^2\sin\alpha)}{s}ds\,d\alpha, \tag{4}$$

$$\varphi(x^1,x^2)=\frac{1}{4\pi^2}\int_0^{2\pi}\int_{-\infty}^{\infty}(\mathcal{R}\varphi)''_{ss}(\alpha,s+x^1\cos\alpha+x^2\sin\alpha)\ln|s|ds\,d\alpha, \tag{5}$$

$$\varphi(x^1,x^2)=-\frac{1}{4\pi^2}\int_0^{2\pi}\int_{-\infty}^{\infty}\frac{(\mathcal{R}\varphi)(\alpha,s+x^1\cos\alpha+x^2\sin\alpha)}{s^2}ds\,d\alpha.$$

The integrals with respect to s are meant in the sense of the Cauchy principal value. Versions (4), (5) of inversion formulas may be directly used for reconstruction of potentials of vector and symmetric 2-tensor fields, respectively. Wherein the derivatives

with respect to s of Radon transforms of corresponding potentials are replaces by longitudinal or transverse ray transforms of vector or tensor fields.

The ray transforms of vector field and inversion formulas. We remind that a vector field $u \in H^k(S^1)$ is potential if there exists a function $\varphi \in H^{k+1}$ (potential) such that $u = \mathrm{d}\varphi$. A field $v \in H^k(S^1(B))$ is solenoidal, if $\delta v \in H^{k-1}(B) = 0$. For every solenoidal vector field v there also exists a potential $\psi \in H^{k+1}(B)$ such that $\mathrm{d}^\perp\psi \in H^k(S^1(B))$ [38]. A vector field $\mathrm{d}h \in C^k(S^1(B))$ is called the harmonic vector field if h is a harmonic function in B.

The (Helmholtz) decomposition of a vector field into potential and solenoidal parts is an important result in vector tomography. The more detailed decomposition into three parts [38], [39], [40], is called the Helmholtz-Hodge theorem. Namely, for every vector field $w \in H^1(S^1(B))$ the unique decomposition

$$w = v + \mathrm{d}h + \mathrm{d}\psi, \quad \delta v = 0, \quad \psi\,|_{\partial B} = 0, \quad \langle v, \nu\rangle\,|_{\partial B} = 0, \tag{6}$$

is valid. Here $\mathrm{d}\psi$ is potential, v is solenoidal, and $\mathrm{d}h$ is harmonic vector field; ν is external normal to the boundary ∂B, $v \in H_0^1(S^1(B))$, $\psi \in H_0^2(B)$.

The vector field $w^s = v + \mathrm{d}h$ is solenoidal (h is harmonic function), and thus (6) may be rewritten as

$$w = w^s + \mathrm{d}\psi, \quad \delta\, w^s = 0, \quad \psi\,|_{\partial B} = 0.$$

Combining $\mathrm{d}h$ and $\mathrm{d}\psi$, $u = \mathrm{d}h + \mathrm{d}\psi = \mathrm{d}(h+\psi) = \mathrm{d}\widetilde{\psi}$, we obtain the other modification of decomposition (6),

$$w = v + \mathrm{d}\widetilde{\psi}, \quad \delta\, v = 0, \quad \langle v, \nu\rangle\,|_{\partial B} = 0.$$

There are only two types of ray transforms, acting on vector fields. They are longitudinal ray transform of vector field $v(x)$,

$$(\mathcal{P}v)(\eta, s) = \int_{-\infty}^{\infty} \big\langle \eta, v(s\xi + t\eta)\big\rangle dt = \int_{-\infty}^{\infty} (\eta^1 v_1 + \eta^2 v_2) dt, \tag{7}$$

and transverse ray transform of the field $u(x)$,

$$(\mathcal{P}^\perp u)(\xi, s) = \int_{-\infty}^{\infty} \big\langle \xi, u(s\xi + t\eta)\big\rangle dt = \int_{-\infty}^{\infty} (\xi^1 u_1 + \xi^2 u_2) dt. \tag{8}$$

As usual ξ is the normal vector, and η is the vector of direction of the straight line, along which the integration is hold.

For vector fields from the class of $\mathcal{C}^k$-potentials we obtain the following form for the decomposition (6),

$$w = \mathrm{d}^\perp\varphi + \mathrm{d}\psi, \quad \psi\,|_{\partial B} = 0, \quad \varphi\,|_{\partial B} = 0,$$

without the harmonic vector field.

A dependence on initial information is emphasized in the formulated below statements for the problems of vector tomography.

1. To reconstruct solenoidal part v of unknown vector field w by its known longitudinal ray transform.

2. To reconstruct potential part u of unknown vector field w by its known transverse ray transform.

3. To reconstruct unknown vector field w completely by its known ray transforms, i.e. by longitudinal and transverse ray transforms.

The properties, kernels, images and relations between ray transforms of vector field and Radon transforms of their potentials are detailed in [41]. It contains also the inversion formulas for the components of a symmetric m-tensor field. Here we state only the inversion formulas giving the potential of a vector field, since this way is one of suitable for reconstruction of discontinuous objects.

The back-projection operator $\mathcal{P}^{\#}_{1tf}$ applied to the image $g(\eta(\alpha), s(x,\alpha))$ of longitudinal ray transform $(\mathcal{P}w)(\eta, s)$ of vector field w, $(\mathcal{P}w) = g$, is defined as

$$\mu(x) = \mathcal{P}^{\#}_{1tf}\big((\mathcal{P}w)(\eta(\alpha), s(x,\alpha))\big)(x).$$

The components are

$$\mu_j(x) = \frac{1}{2\pi}\int_0^{2\pi} \eta^j (\mathcal{P}w)(\eta(\alpha), s(x,\alpha))d\alpha, \quad j = 1,2, \tag{9}$$

$s(x,\alpha) = x^1\cos\alpha + x^2\sin\alpha$. As a result of the action of this operator we have the solenoidal vector field μ for any field w. The back-projection operator applied to the transverse ray transform $h(\xi(\alpha), s(x,\alpha)) = (\mathcal{P}^{\perp}w)(\xi, s)$ of a field w gives the potential vector field λ,

$$\lambda(x) = \big(\mathcal{P}^{\perp}\big)^{\#}_{1tf}\big((\mathcal{P}^{\perp}w)(\xi(\alpha), s(x,\alpha))\big)(x) \tag{10}$$

with components

$$\lambda_j(x) = \frac{1}{2\pi}\int_0^{2\pi} \xi^j (\mathcal{P}^{\perp}w)(\xi(\alpha), s(x,\alpha))d\alpha, \quad j = 1,2. \tag{11}$$

In terms of the vector fields μ, λ we can write simple inversion formulas,

$$v = (-\Delta)^{1/2}\mu, \quad u = (-\Delta)^{1/2}\lambda,$$

where v is solenoidal part of vector field w, and u is potential part of w.

With usage of the relations between the ray transforms of a vector field and the Radon transforms of its potential one can get inversion formulas reconstructing the potential of the vector field by its known longitudinal (transverse) ray transform. We state, for example, the inversion formulas for the potential φ of solenoidal part v of a field w,

$$\varphi(x^1, x^2) = -\frac{1}{4\pi^2}\int_0^{2\pi}\int_{-\infty}^{\infty} \frac{(\mathcal{P}w)(\alpha, s + x^1\cos\alpha + x^2\sin\alpha)}{s} ds\, d\alpha,$$

$$\varphi(x^1, x^2) = \frac{1}{4\pi^2}\int_0^{2\pi}\int_{-\infty}^{\infty} (\mathcal{P}w)'_s(\alpha, s + x^1\cos\alpha + x^2\sin\alpha)\ln(s) ds\, d\alpha.$$

On the base of the reconstructed potential φ the solenoidal field $v = \mathrm{d}^{\perp}\varphi$ may be constructed easily. For this we need to differentiate the potential φ and then to find the components $v_1 = -\partial\varphi/\partial x^2$, $v_2 = \partial\varphi/\partial x^1$ of the field v. The same inversion formulas may be used also for the reconstruction of the potential ψ of the potential field $\mathrm{d}\psi$. Then we find the components $u_1 = \partial\psi/\partial x^1$, $u_2 = \partial\psi/\partial x^2$ of the field u.

2 Indicators of inhomogeneity and breaks

The aim of the section is to construct the operators of indicator of breaks allowing to distinguish a set of break points by known Radon or ray transforms. We use differential operators of tensor analysis, integral operators of angular moment and back-projection for solving the problem.

2.1 The operator of indicator of function breaks

Let's consider a problem clarifying the idea of application of differential operators for reconstruction of breaks of a function. For this purpose a behavior of the breaks indicator for the characteristic function of the circle is investigated,

$$\varphi(x,y) = \begin{cases} C, & x^2+y^2<1, \\ 0, & \text{otherwise}, \end{cases} \tag{12}$$

where $C > 0$ is a constant. Radon transform of function (12) is known, $(\mathcal{R}\varphi)(\xi, s) = 2C\sqrt{1-s^2}$. A distance from a line, passing through a point $(x, y) \in B$ and defined by the normal vector $\xi = (\cos\alpha, \sin\alpha)$, is equal to $s = |x\cos\alpha + y\sin\alpha|$. Suppose $x = \rho\cos\gamma$, $y = \rho\sin\gamma$ for $0 \le \gamma < 2\pi$, $\rho < 1$. Then $\sqrt{1-s^2} = \sqrt{1-\rho^2\cos^2(\alpha-\gamma)}$. An application of the back-projection operator $\mathcal{R}^{\#}$ and variables change $\alpha = \pi/2+\gamma-\chi$ give

$$\mu = \frac{1}{\pi}\int\limits_0^{2\pi}\sqrt{1-\rho^2\cos^2(\alpha-\gamma)}d\alpha.$$

Properties of the integrand imply that the last expression can be written in the form

$$\mu = \frac{4C}{\pi}\mathbf{E}(\rho) = \frac{4C}{\pi}\int\limits_0^{\pi/2}\sqrt{1-\rho^2\sin^2\chi}d\chi, \tag{13}$$

where the integral is complete elliptic integral of the second kind $\mathbf{E}(\rho)$,

$$\mathbf{E}(\rho) = \int\limits_0^{\pi/2}\sqrt{1-\rho^2\sin^2\chi}d\chi.$$

By means of its series expansion with respect to ρ, $0 \le \rho \le 1$, [42]

$$\begin{aligned}\mathbf{E}(\rho) = \; & 1 + \frac{1}{2}\Big(\ln\frac{4}{\sqrt{1-\rho^2}} - \frac{1}{1\cdot 2}\Big)(1-\rho^2) + \\ + \; & \frac{1^2\cdot 3}{2^2\cdot 4}\Big(\ln\frac{4}{\sqrt{1-\rho^2}} - \frac{2}{1\cdot 2} - \frac{1}{3\cdot 4}\Big)(1-\rho^2)^2 + \\ + \; & \frac{1^2\cdot 3^2\cdot 5}{2^2\cdot 4^2\cdot 6}\Big(\ln\frac{4}{\sqrt{1-\rho^2}} - \frac{2}{1\cdot 2} - \frac{2}{3\cdot 4} - \frac{1}{5\cdot 6}\Big)(1-\rho^2)^3 + ...\end{aligned} \tag{14}$$

we obtain that $\mathbf{E}(\rho) \to 1$ at $\rho \to 1$, and hence $\mu \to 4C/\pi$ at $\rho \to 1$. The same conclusion can be made if we suppose $\rho = 1$ in (13). Then the integral is expressed in terms of elementary functions, and we obtain the same value for μ which was obtained with usage of the limit transition.

Now we investigate a behavior of the partial derivatives $\partial\mu/\partial x$, $\partial\mu/\partial y$ and the derivative with respect to the normal, $\partial\mu/\partial\rho$,

$$\frac{\partial\mu}{\partial t} = -\frac{4Ct}{\pi} I(\rho), \quad \text{at } \; t = x, y, \rho.$$

The integral $I(\rho) = \displaystyle\int_0^{\pi/2} \frac{\sin^2\chi}{\sqrt{1-\rho^2\sin^2\chi}} d\chi$, included in the last equation, is expressed in terms of complete elliptic integrals of the first

$$\mathbf{K}(\rho) = \int_0^{2\pi} \frac{d\chi}{\sqrt{1-\rho^2\sin^2\chi}}.$$

and the second $\mathbf{E}(\rho)$ kind (13) as follows,

$$I(\rho) = -\frac{\mathbf{E}(\rho)}{\rho^2} + \frac{\mathbf{K}(\rho)}{\rho^2}.$$

Referring to the series expansion of the function $\mathbf{K}(\rho)$ [42],

$$\begin{aligned}\mathbf{K}(\rho) = \; & \ln\frac{4}{\sqrt{1-\rho^2}} + \Big(\frac{1}{2}\Big)^2\Big(\ln\frac{4}{\sqrt{1-\rho^2}} - \frac{2}{1\cdot 2}\Big)(1-\rho^2) + \\ + \; & \Big(\frac{1\cdot 3}{2\cdot 4}\Big)^2\Big(\ln\frac{4}{\sqrt{1-\rho^2}} - \frac{2}{1\cdot 2} - \frac{2}{3\cdot 4}\Big)(1-\rho^2)^2 + \\ + \; & \Big(\frac{1\cdot 3\cdot 5}{2\cdot 4\cdot 6}\Big)^2\Big(\ln\frac{4}{\sqrt{1-\rho^2}} - \frac{2}{1\cdot 2} - \frac{2}{3\cdot 4} - \frac{2}{5\cdot 6}\Big)(1-\rho^2)^3 + ...,\end{aligned} \tag{15}$$

we obtain that $\mathbf{K}(\rho)$ at $\rho \to 1$ has the logarithmic singularity, namely $\mathbf{K}(\rho) \sim \ln 2\sqrt{2} - \ln\sqrt{1-\rho} \to +\infty$. Hence $I(\rho) \sim -\ln(1-\rho) \to +\infty$ at $\rho \to 1$, and thereby at $\rho \to 1$ we have

$$\begin{aligned}\frac{\partial\mu}{\partial x} &= -\frac{4}{\pi} x I(\rho) \sim \frac{4}{\pi} x \ln(1-\rho) \to \mp\infty, \; x0, \\ \frac{\partial\mu}{\partial y} &= -\frac{4}{\pi} y I(\rho) \sim \frac{4}{\pi} y \ln(1-\rho) \to -\infty, \; y \ne 0, \\ \frac{\partial\mu}{\partial\rho} &= -\frac{4}{\pi} \rho I(\rho) \sim \frac{4}{\pi} \rho \ln(1-\rho) \to -\infty.\end{aligned}$$

$$\begin{aligned}
&\frac{\partial \mu}{\partial t} = -\frac{4C}{\pi} t I(\rho) \sim \frac{4C}{\pi} t \ln(1-\rho) \to \begin{cases} -\infty, \, t > 0, \\ +\infty, \, t < 0, \end{cases} \quad t = x, y, \\
&\frac{\partial \mu}{\partial \rho} = -\frac{4C}{\pi} \rho I(\rho) \sim \frac{4C}{\pi} \rho \ln(1-\rho) \to -\infty.
\end{aligned} \tag{16}$$

The tendency to $\pm\infty$ of the partial derivatives $\partial\mu/\partial x$, $\partial\mu/\partial y$ allows to use the operator $|\mathrm{d}(\cdot)|$ as the break indicator of a scalar field. Based on (16) we obtain that the operator $|\mathrm{d}(\cdot)|$ has the logarithmic singularity at the boundary, and

$$|\mathrm{d}\mu| = \sqrt{\Big(\frac{\partial \mu}{\partial x}\Big)^2 + \Big(\frac{\partial \mu}{\partial y}\Big)^2} \to \infty$$

at $\rho \to 1$.

2.2 The indicators of breaks for vector fields

Starting from C-potential

$$\varphi(x,y) = \begin{cases} \big(1 - x^2 - y^2\big) & , \quad \text{at} \quad x^2 + y^2 < 1 \\ 0 & , \quad \text{at} \quad x^2 + y^2 \geq 1 \end{cases}$$

and its Radon transform $\big(\mathcal{R}\varphi\big)(\xi, s) = 4\big(1 - s^2\big)^{3/2}/3$, for $|s| < 1$, and $\big(\mathcal{R}\varphi\big)(\xi, s) = 0$ for $|s| \geq 1$, a partial derivative of $\mathcal{R}\varphi$ with respect to s,

$$\frac{\partial (\mathcal{R}\varphi)(\xi, s)}{\partial s} = -4s\sqrt{1 - s^2}$$

is calculated easily. The properties of ray transforms show that this derivative is both the longitudinal ray transform of the solenoidal field $v = (2y, -2x)$, and the transverse ray transform of the field $\mathrm{d}\varphi = u = (-2x, -2y)$.

For definiteness the longitudinal ray transform of the potential field v will be considered. As $s = x\cos\alpha + y\sin\alpha$ then, assuming $x = \rho\cos\gamma$, $y = \rho\sin\gamma$, we obtain $s = \rho\cos(\alpha - \gamma)$, $\sqrt{1 - s^2} = \sqrt{1 - \rho^2\cos^2(\alpha - \gamma)}$. Thus the expressions for the components of vector field μ, obtained as a result of application of the back-projection operator, accept the form

$$\begin{aligned}
\mu_1(x,y) &= \frac{2}{\pi} \int_0^{2\pi} \sin\alpha\big(\rho\cos(\alpha - \gamma)\big)\sqrt{1 - \rho^2\cos^2(\alpha - \gamma)}\, d\alpha, \\
\mu_2(x,y) &= -\frac{2}{\pi} \int_0^{2\pi} \cos\alpha\big(\rho\cos(\alpha - \gamma)\big)\sqrt{1 - \rho^2\cos^2(\alpha - \gamma)}\, d\alpha.
\end{aligned}$$

Changes of variables $\beta = \alpha - \gamma$ and $\chi = \pi/2 - \beta$ after obvious converting lead to the formulas

$$\begin{aligned}
\mu_1(x,y) &= \frac{8y}{\pi} \int_0^{\pi/2} \sin^2\chi\sqrt{1 - \rho^2\sin^2\chi}\, d\chi = \frac{8y}{\pi}\, \mathbf{I}_1(\rho) \\
\mu_2(x,y) &= -\frac{8x}{\pi} \int_0^{\pi/2} \sin^2\chi\sqrt{1 - \rho^2\sin^2\chi}\, d\chi = -\frac{8x}{\pi}\, \mathbf{I}_1(\rho)
\end{aligned} \tag{17}$$

The integral $\mathbf{I}_1(\rho)$ at the right-hand sides of (17) is expressed

$$\mathbf{I}_1(\rho) = \frac{1-\rho^2}{3\rho^2} F(\pi/2, \rho) - \frac{1-2\rho^2}{3\rho^2} E(\pi/2, \rho)$$

through the elliptic integrals of the first and the second kind,

$$F(\delta, \rho) = \int_0^\delta \frac{d\alpha}{\sqrt{1-\rho^2 \sin^2 \alpha}}, \quad E(\delta, \rho) = \int_0^\delta \sqrt{1-\rho^2 \sin^2 \alpha} d\alpha,$$

respectively. As $F(\pi/2, \rho) = \mathbf{K}(\rho)$, $E(\pi/2, \rho) = \mathbf{E}(\rho)$, where $\mathbf{K}$ and $\mathbf{E}$ are complete elliptic integrals of the first and the second kind, so

$$\mathbf{I}_1(\rho) = \frac{1-\rho^2}{3\rho^2} \mathbf{K}(\rho) - \frac{1-2\rho^2}{3\rho^2} \mathbf{E}(\rho)$$

As $\mathbf{E}(\rho) \to 1$, $(1-\rho^2)\mathbf{K}(\rho) \to 0$ at $\rho \to 1$, so we obtain $\mathbf{I}_1(\rho) \to 1/3$, and

$$\mu_1 \to 8 \sin \gamma / 3\pi, \quad \mu_2 \to -8 \cos \gamma / 3\pi \quad \text{at } \rho \to 1.$$

These conclusions are the consequences of series expansions (14), (15). Substituting $\rho = 1$ to the formulas (17) we obtain integrals which are expressed in terms of elementary functions. Further simple calculations give the same expressions for μ_1, μ_2 that were obtained with usage of the limit transition.

Below the value of

$$\mathbf{I}_2(\rho) = \int_0^{\pi/2} \frac{\sin^4 \chi \, d\chi}{\sqrt{1-\rho^2 \sin^2 \chi}}$$

will be necessary. A corresponding indefinite integral is

$$\mathbf{I}_2(\chi, \rho) = \frac{\sin \chi \cos \chi}{3\rho^2} \sqrt{1-\rho^2 \sin^2 \chi} + \frac{2+\rho^2}{3\rho^4} F(\chi, \rho) - \frac{2(1+\rho^2)}{3\rho^4} E(\chi, \rho).$$

The properties of trigonometric functions and elliptic integrals give

$$\mathbf{I}_2(\rho) = \frac{2+\rho^2}{3\rho^4} \mathbf{K}(\rho) - \frac{2(1+\rho^2)}{3\rho^4} \mathbf{E}(\rho). \tag{18}$$

By means of representation (18) and series expansions for $\mathbf{K}(\rho)$ and $\mathbf{E}(\rho)$ we investigate a behavior of the value $\mathbf{I}_2$ at $\rho \to 1$ below. At first, we note that the complete elliptic integral of the 1-st kind $\mathbf{K}(\rho) \sim \ln(4/\sqrt{1-\rho^2}) \sim \ln 2\sqrt{2} - \ln \sqrt{1-\rho} \to +\infty$ at $\rho < 1$, $\rho \to 1$. Hence by using (18) we obtain $\mathbf{I}_2(\rho) \to +\infty$ at $\rho < 1$, $\rho \to 1$. It was established above that $\mathbf{I}_1(\rho) \to 1/3$, so $d\,\mathbf{I}_1(\rho)/d\rho = -\rho \mathbf{I}_2(\rho)$, and

$$\begin{aligned} &\frac{\partial \mu_1}{\partial x} = -\frac{8xy}{\pi} \mathbf{I}_2(\rho), && \frac{\partial \mu_1}{\partial y} = \frac{8}{\pi} \mathbf{I}_1(\rho) - \frac{8y^2}{\pi} \mathbf{I}_2(\rho), \\ &\frac{\partial \mu_2}{\partial x} = -\frac{8}{\pi} \mathbf{I}_1(\rho) + \frac{8x^2}{\pi} \mathbf{I}_2(\rho), && \frac{\partial \mu_2}{\partial y} = \frac{8xy}{\pi} \mathbf{I}_2(\rho). \end{aligned} \tag{19}$$

It implies that at $\rho < 1$, $\rho \to 1$

$$\begin{aligned} &\frac{\partial \mu_1}{\partial x} \to -\infty, \quad x \neq 0,\ y \neq 0, \qquad \frac{\partial \mu_1}{\partial y} \to -\infty, \quad y \neq 0, \\ &\frac{\partial \mu_2}{\partial x} \to +\infty, \quad x \neq 0, \qquad \frac{\partial \mu_2}{\partial y} \to +\infty, \quad x \neq 0,\ y \neq 0. \end{aligned} \tag{20}$$

Hence the behavior of partial derivatives at approaching a point inside the disk to the circle is established.

A behavior of derivatives $\partial\mu_1/\partial\rho$, $\partial\mu_2/\partial\rho$ of the vector field μ with respect to the normal to the circle, $\rho \to 1$, will be considered now. Since

$$\frac{\partial \mu_1}{\partial \rho} = \frac{8\sin\gamma}{\pi}\mathbf{I}_1(\rho) - \frac{8\rho^2\sin\gamma}{\pi}\mathbf{I}_2(\rho), \quad \frac{\partial \mu_2}{\partial \rho} = -\frac{8\cos\gamma}{\pi}\mathbf{I}_1(\rho) + \frac{8\rho^2\cos\gamma}{\pi}\mathbf{I}_2(\rho),$$

then $\partial\mu_1/\partial\rho \to -\infty$, $\partial\mu_2/\partial\rho \to +\infty$. At $x \neq 0$, $y \neq 0$ partial derivatives $\partial\mu_1/\partial x$, $\partial\mu_1/\partial y$ tend to $-\infty$, and $\partial\mu_2/\partial x$, $\partial\mu_2/\partial y$ tend to $+\infty$ at $\rho < 1$, $\rho \to 1$.

As indicators of breaks of a vector field may be chosen, in particular, such operators as $|\mathrm{d}\mu|$, $|\delta\mu|$, $|\delta^\perp\mu|$. Really, based on (19), (20) we obtain

$$|\nabla\mu| = \left(\left(\frac{\partial\mu_1}{\partial x}\right)^2 + \left(\frac{\partial\mu_1}{\partial y}\right)^2 + \left(\frac{\partial\mu_2}{\partial x}\right)^2 + \left(\frac{\partial\mu_2}{\partial y}\right)^2\right)^{1/2} \to \infty,$$

at $\rho < 1$, $\rho \to 1$,

$$|\delta^\perp\mu| = \left|\frac{\partial\mu_2}{\partial x} - \frac{\partial\mu_1}{\partial y}\right| \to \infty,$$

$\rho < 1$, $\rho \to 1$. These operators have logarithmic singularities near the boundary due to the behavior of partial derivatives.

The operator δ and corresponding the indicator of breaks $|\delta\mu|$ are interesting. Expressions (19) yield

$$\delta\mu = \frac{\partial\mu_1}{\partial x} + \frac{\partial\mu_2}{\partial y} = -\frac{8xy}{\pi}\mathbf{I}_2(\rho) + \frac{8xy}{\pi}\mathbf{I}_2(\rho) = 0, \quad \rho < 1.$$

and so the field μ is solenoidal. Thus the operator δ "cancels" the field μ in the circle B. Nevertheless numerical experiments show good quality of the visualization of breaks of vector fields and breaks of their derivatives. Likewise the operator $\delta^\perp$ acts on the image of back-projection operator acting on the transverse ray transform of a potential vector field. It should be noted that

$$\delta^\perp\mu \equiv \frac{\partial\mu_2}{\partial x} - \frac{\partial\mu_1}{\partial y} = -\frac{16}{\pi}\mathbf{I}_1(\rho) + \frac{8\rho^2}{\pi}\mathbf{I}_2(\rho).$$

2.3 A behavior of operators of inhomogeneity and breaks indicators. Simulation

Test 2.1 demonstrates a behavior of the Vainberg operator and the operator of "gradient module". In the second test 2.2 an action of different operators of breaks

indicator is demonstrated. They acts on the longitudinal ray transform of discontinuous solenoidal vector field.

Test 2.1. Discontinuous function and function with discontinuous first derivatives. The Vainberg operator does not distinguish between breaks of a function and breaks of its first derivatives. This operator consists in the following sequence of operations,

$$\mathcal{R}\varphi \to \frac{\partial^2}{\partial s^2}\big(\mathcal{R}\varphi\big) \to \mathcal{R}^{\#}(\frac{\partial^2}{\partial s^2}(\mathcal{R}\varphi)) = g(x,y).$$

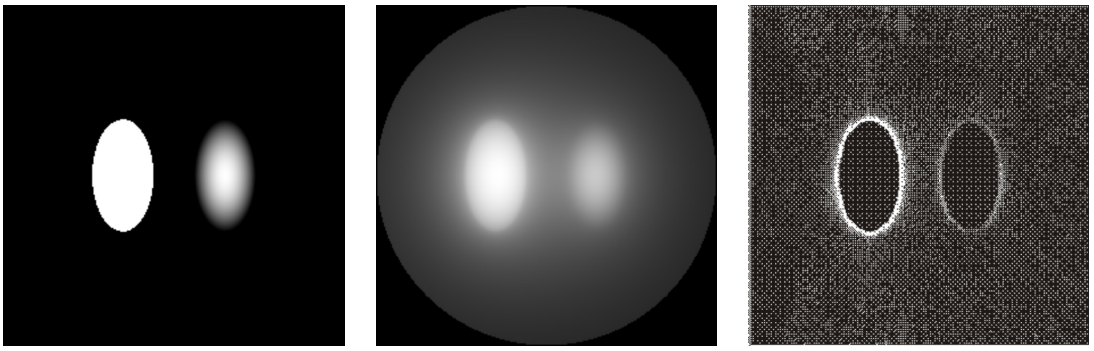

a) $\mathcal{C}^{-1}\&\mathcal{C}^0$ b) BP operator c) Vainberg operator

Fig. 1.

The operator "gradient module" is applied to the back-projection operator and consists in the following sequence of operations,

$$\mathcal{R}\varphi \to \mathcal{R}^{\#}(\mathcal{R}\varphi) \to |\nabla(\mathcal{R}^{\#}(\mathcal{R}f))| = g(x,y).$$

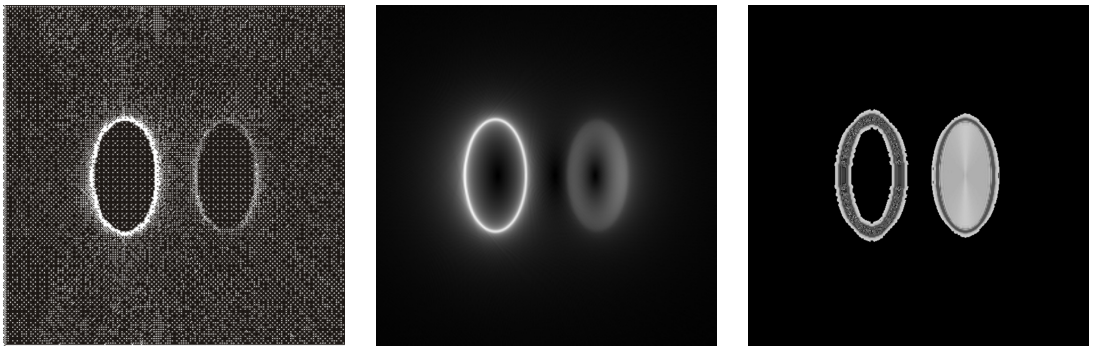

a) Vainberg operator b) Gradient module c) GM twice

Fig. 2.

The operator of double "gradient module", starting with the last function g of the previous sequence (gradient module), is looks like

$$g(x,y) \to \nabla g \to |\nabla g| = h(x,y).$$

Conclusions are obvious. The Vainberg operator does not distinguish between breaks of the function and breaks of its first derivatives. From a mathematical point of view, this operator approximates δ-function arising at the line of breaks after double differentiation with respect to s. Operator "gradient module" acts more carefully. The

figure shows that there is no singularities at the continuous function with breaks in derivatives, but breaks of discontinuous function are visualized distinctly.

Test 2.2. Discontinuous solenoidal vector field. A vector field is constructed based on the potential $\varphi(x,y) = h - h\sqrt{x^2+y^2}/R$ at $x^2+y^2 < R^2$ and $\varphi(x,y) = 0$ at $x^2+y^2 \geq R^2$,

$$v = (v_1, v_2) = \Big(\frac{h}{R}\frac{y}{\sqrt{x^2+y^2}}, -\frac{h}{R}\frac{x}{\sqrt{x^2+y^2}}\Big).$$

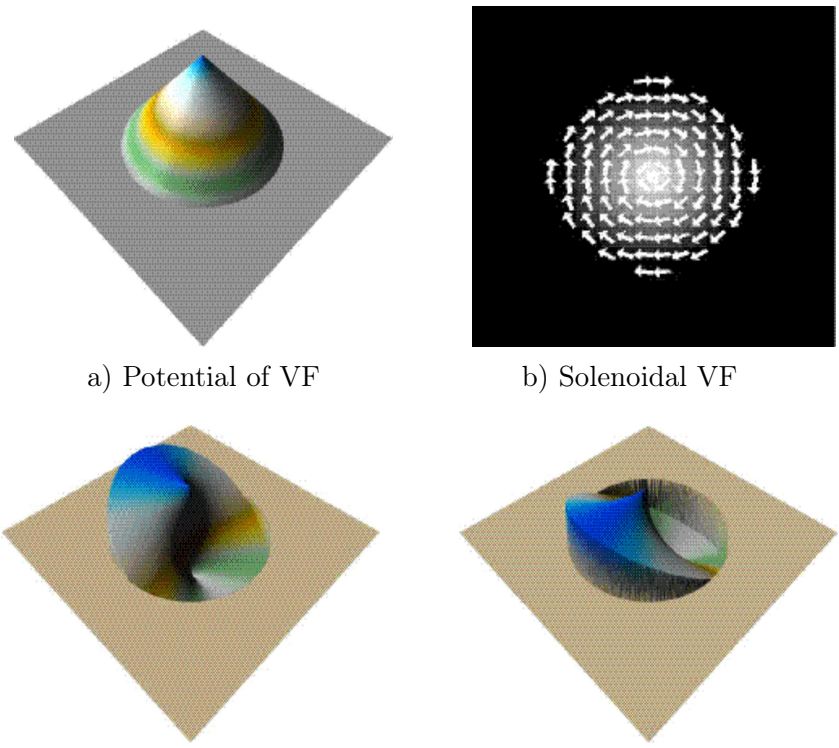

a) Potential of VF b) Solenoidal VF

c) Component 1 d) Component 2

Fig. 3.

The longitudinal ray transform of solenoidal vector field under consideration is

$$(\mathcal{P}v)(\eta, s) = -\frac{h}{R} s \ln \frac{R+\sqrt{R^2-s^2}}{R-\sqrt{R^2-s^2}}.$$

Figure 4 shows the results of action of different operators of breaks indicator. The breaks indicator operators of a discontinuous solenoidal vector field is described by the following sequences of simple operators.

$$\mathcal{P}v \to \mathcal{P}^{\#}_{1tf}(\mathcal{P}v) = (\mu_1, \mu_2) \to \nabla\mu = (\nu_{ij}) \to |\nu(x,y)|.$$

$$\mathcal{P}v \to \mathcal{P}^{\#}_{1tf}(\mathcal{P}v) = (\mu_1, \mu_2) \to |\operatorname{div}\mu(x,y)|.$$

$$\mathcal{P}v \to \frac{\partial}{\partial s}(\mathcal{P}v) = g(\eta, s) \to |\mathcal{P}^{\#}_{f}\big(\frac{\partial}{\partial s}(\mathcal{P}v)\big)(x,y)|.$$

$$\mathcal{P}v \to \frac{\partial}{\partial s}(\mathcal{P}v) = g(\eta, s) \to |\mathcal{P}^{\#}_{2tf}\big(\frac{\partial}{\partial s}(\mathcal{P}v)\big)(x,y)|.$$

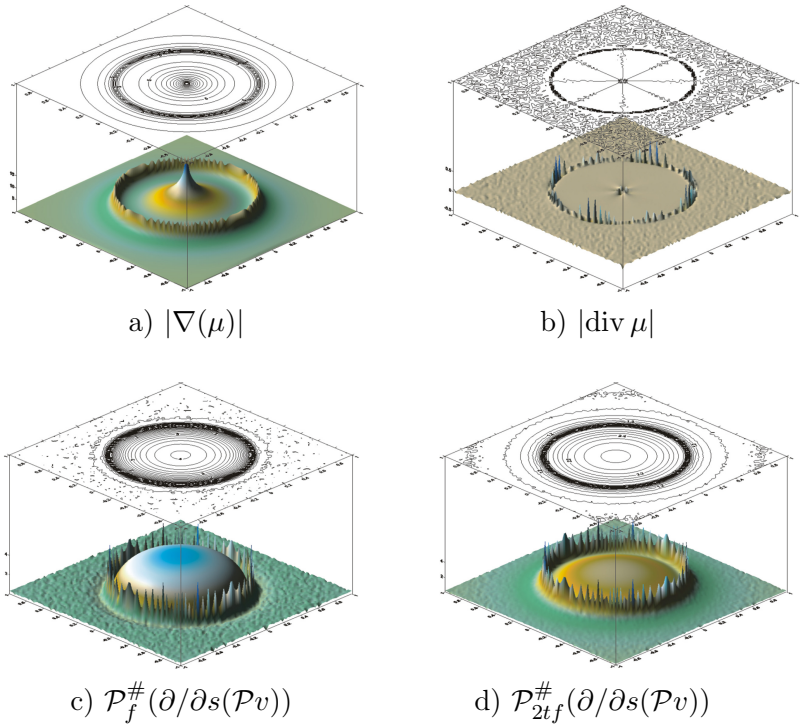

a) $|\nabla(\mu)|$ b) $|\mathrm{div}\,\mu|$

c) $\mathcal{P}_f^{\#}(\partial/\partial s(\mathcal{P}v))$ d) $\mathcal{P}_{2tf}^{\#}(\partial/\partial s(\mathcal{P}v))$

Fig. 4.

As it is shown at the figure the operators $|\nabla(\mu)|$ and $|\mathrm{div}\,\mu|$ allocate the isolated singularity in the origin. But if at first we apply differentiation with respect to s, and after that back-projection operator, this singular point disappears. The line of breaks at all four pictures of the figure is visualized distinctly.

3 Algorithms for breaks reconstruction of a function or its first derivatives

Initial data for the problem of breaks reconstruction of a function or its first derivatives are discrete values of the Radon transform of the function. It should be remind the breaks of the first type are considered only. Besides the Radon transform, the other operators are intended for the problem of reconstruction of geometrical objects with not empty singular support solving. The first step consists in visualization of a set of breaks or singular support points.

3.1 A description of algorithms

A visualization of a set of singular support points of a function

Steps and discretization procedures of a visualization algorithm of a set of singular support points of a function. The algorithm is based on the gradient module operator and includes following elements:

– 1. Discretization of the Radon transform values (2) by s, α for a test function.
– 2. An approximate calculation of the integral (2) of a test function for fixed s, α.
– 3. An approximate calculation of values of the back-projection operator (BPO).

– 4. An application of the operator $|\nabla \cdot|$ to the values of BPO. The operator may be applied repeatedly.
– 5. A visualization of obtained function.

Steps and discretization procedures of a visualization algorithm of a set of singular support points of a function. The algorithm is based on the Vainberg module operator and includes just the same elements as above except point 3, 4:
– 3. An application of the operator of double differentiation with respect to s to the values of the Radon transform. The operator may be applied repeatedly.
– 4. An approximate calculation of values of BPO.

Let,s describe basic procedures.

The discretization of variables α, s**.** Specifying an integer L we form discrete sequences

$$\begin{aligned} &\alpha_k, && k = 0, \dots, 4L-1, && \alpha_0 = 0, && \Delta\alpha = \pi/(2L); \\ &s_i, && i = -L+1, \dots, L-1, && s_0 = 0, && \Delta s = 1/L. \end{aligned}$$

The values α_k, s_i define a line $L_{\xi_k s_i}$ of the integration, $\xi_k = (\cos\alpha_k, \sin\alpha_k)$ is the normal vector of $L_{\xi_k s_i}$. In the numerical tests a discrete grid of a size 256×128 for α, s is used.

An approximate calculation of the Radon transform values. For calculating the integrals along straight lines we use the five-point quadrature Newton-Cotes formula of the reserved type

$$\int_{t_0}^{t_4} F(t)\,dt \approx \frac{\Delta t}{45}\big(14\,F(t_0) + 64\,F(t_1) + 24\,F(t_2) + 64\,F(t_3) + 14\,F(t_4)\big). \tag{21}$$

The values α_k, s_i define a line $L_{\xi_k s_i} = \{x \in \mathbb{R}^2 \mid \xi_k^1 x^1 + \xi_k^2 x^2 = s_i\}$ of the integration. The vector $(-\sin\alpha_k, \cos\alpha_k)$ is the direction vector of the line $L_{\xi_k s_i}$. The integration from a point $(s_i\cos\alpha_k + \sqrt{1-s_i^2}\sin\alpha_k,\ s_i\cos\alpha_k - \sqrt{1-s_i^2}\sin\alpha_k)$ to a point $(s_i\cos\alpha_k - \sqrt{1-s_i^2}\sin\alpha_k,\ s_i\cos\alpha_k + \sqrt{1-s_i^2}\sin\alpha_k)$ is implemented. At each step of integration the condition of the ray to be output of the domain of integration is controlled.

An approximate calculation of the values of the back-projection operator for the Radon transform and its derivatives $g(\alpha, s) = \partial^{2n}(\mathcal{R}f)/\partial s^{2n}(\alpha, s)$ are calculated in the square $[-4, 4]^2$. The discrete grid with a step size $\Delta x^1 = \Delta x^2 = 1/64$ for calculating the BPO image is used. We obtain discrete sequences

$$\begin{aligned} &x_l^1, && l = 0, \dots, 512, && x_0^1 = -4; \\ &x_m^2, && m = 0, \dots, 512, && x_0^2 = -4. \end{aligned}$$

Specifying an integer N_γ we form discrete sequences of angles $\gamma_j = 2\pi j/N_\gamma$, $j = 0, ..., N_\gamma - 1$, by which the numerical integration is performed. In our numerical tests we use $N_\gamma = 256$ so that $\Delta\gamma = \Delta\alpha$. For a point $x_{lm} = (x_l^1, x_m^2)$ and an angle γ_j we obtain $s_{lmj} = x_l^1\cos\gamma_j + x_m^2\sin\gamma_j$.

If $|s_{lmj}| \leqslant 1$, then the value $(\mathcal{R}f)(\gamma_j, s_{lmj})$ (its derivative $g(\gamma_j, s_{lmj})$) is defined as the linear interpolation by $(\mathcal{R}f)(\alpha_i, s_k)$ and $(\mathcal{R}f)(\alpha_i, s_{k+1})$ (respectively, $g(\alpha_i, s_k)$ and $g(\alpha_i, s_{k+1})$) with the properties $\alpha_i = \gamma_j$ and $s \in [s_k, s_{k+1}]$.

If $|s_{lmj}| > 1$, we suppose $(\mathcal{R}f)(\gamma_j, s_{lmj}) = 0$.

The value of BPO at the point x_{lm} is obtained by numerical integration of $(\mathcal{R}f)(\gamma_j, s_{lmj})$ with respect to γ_i with usage of the formula (21).

An approximate calculation of the values of BPO for the ray transforms of tensor fields and their derivatives are performed similarly.

An application of the operator $|\nabla \cdot|$ to the values of BPO. Differentiation with respect to x^1, x^2 is done by means of central difference scheme

$$h'_t(t_i) = \frac{h(t_{i+1}) - h(t_{i-1})}{t_{i+1} - t_{i-1}}.$$

An application of the operator of double differentiation with respect to s is implemented with usage of the central difference scheme

$$g''_{ss}(s_i) = \frac{g(s_{i+1}) - 2g(s_i) + g(s_{i-1})}{(s_i - s_{i-1})^2}.$$

A visualization algorithms of a set of points of a vector field singular support.

Steps and discretization procedures of a visualization algorithm of a set of points of singular support of a vector field with usage of the operators of inner differentiation and divergence includes the following elements:

– 1. Discretization of the longitudinal (7) or transverse (8) ray transform values by s, α for a test vector field.

– 2. An approximate calculation of the integrals (7) or (8) of a test vector field for fixed s, α.

– 3. An approximate calculation of values of the back-projection operator.

– 4. An application of the operators of inner differentiation and divergence to the values of the back-projection operator.

– 5. A visualization of the obtained function.

Steps and discretization procedures of a visualization algorithm of a set of points of singular support of a vector field with usage of the Vainberg operator includes the same elements excepts the points 3 and 4:

– 3. An application of the operator of double differentiation with respect to s many times as needed to the values of the ray transform.

– 4. An approximate calculation of values of the back-projection operator.

All steps and discretization procedures of the visualization algorithms for a set of points of singular support of the vector field are similar to the scalar case.

3.2 An action of the operators of breaks indicator on the Radon transform of a discontinuous function

We assume the following agreement. The values of all used below potentials and corresponding vector fields vanish outside of a domain B, which is a circle of radius $R < 1$. Therefore the formulas are given only for variables that lie inside of D. The formulas for the Radon transform and the ray transforms are given for s, $-R \leq s \leq R$. The transforms are equal to 0 for $|s| \geqslant R$. The results of numerical experiments are represented below.

Test 3.1. A dependence of quality of reconstruction of a function breaks from noisy data. First test contains the results of reconstruction of the set of break points of a piecewise constant function by its known Radon transform. The functions is shown at Fig. 5 (a). The operator $|\nabla(\,\cdot\,)|$ is used.

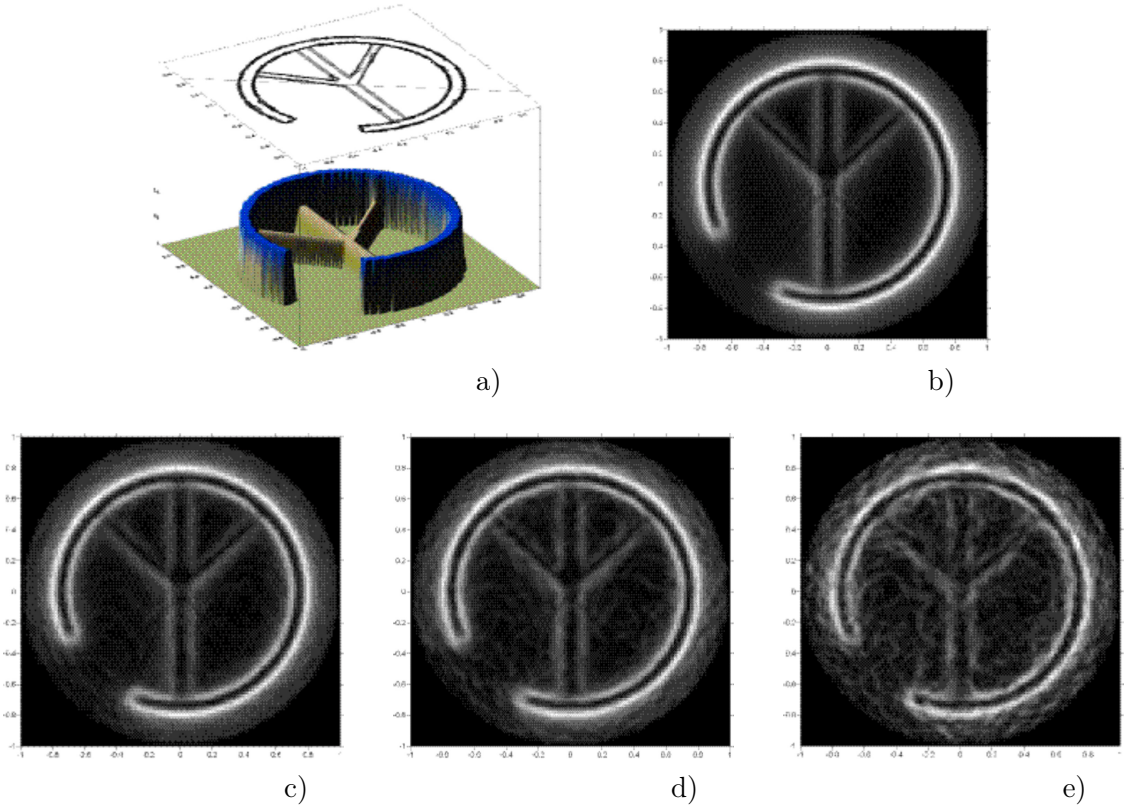

a) b) c) d) e)

Fig. 5.
The piecewise constant function (a) and visualizations of its breaks: exact data (b); data with the noise level in 5% (c); 10% (d) and 20% (e).

A uniform distributed error with various levels is carried in the data. It can be concluded that outlines of breaks are visualized, despite the very significant level of error 20%.

Test 3.2. An action of the Vainberg operator and the gradient module operator (GMO) on the functions of varying degrees of smoothness.

The Vainberg operator acting on the Radon transform of function φ can be represented as a scheme $(\mathcal{R}\varphi)(\xi,s) \to g(\xi,s) := \partial^2/\partial s^2(\mathcal{R}\varphi)(\xi,s) \to \psi(x,y) := (\mathcal{R}^{\#}g)(x,y)$. It may be said that a single action of the Vainberg operator (in a sense smoothness) is equivalent to a twice action of GMO.

An elementary phantom φ is a "λ-parabola" with an elliptical support,

$$\varphi(x,y) = \begin{cases} C(1-t^2)^{\lambda} & , \quad t \le 1, \\ 0 & , \quad t > 1, \end{cases}$$

where

$$t^2 = \frac{((x-x_0)\cos\beta + (y-y_0)\sin\beta)^2}{a^2} + \frac{(-(x-x_0)\sin\beta + (y-y_0)\cos\beta)^2}{b^2},$$

and the Radon transform, $\lambda > 0$ [43],

$$(\mathcal{R}\varphi)(s,\phi) = \frac{\sqrt{\pi}abC\Gamma(\lambda+1)}{|\zeta|\Gamma(\lambda+3/2)}\left(1-\frac{(s-s_0)^2}{\zeta^2}\right)^{\lambda+1/2}.$$

Here $s_0 = -x_0\sin\phi + y_0\cos\phi$, $\zeta^2 = a^2\sin^2(\phi-\beta) + b^2\cos^2(\phi-\beta)$. A complex phantom is made up from the elementary phantoms. It is similar to the Shepp-Logan phantom by the contours and is named as the "potential 2" (Pot2).

Figure 6 presents an action of the back-projection operator applied to the Radon transform of the potential 2. The degree of smoothness of the potential is determined by the parameter λ.

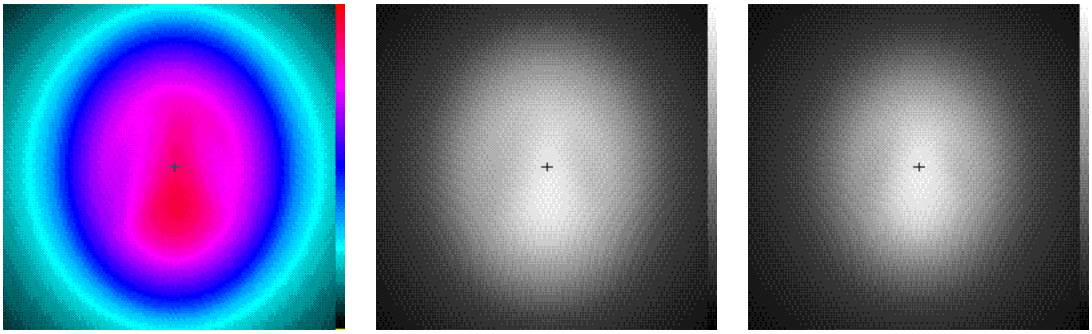

a) $\lambda = 0.5$ b) $\lambda = 1$ c) $\lambda = 2$

Fig. 6.
An application of BPO to the Radon transform of Pot2.

Figure 7 presents the results of application of the Vainberg operator to the Radon transform.

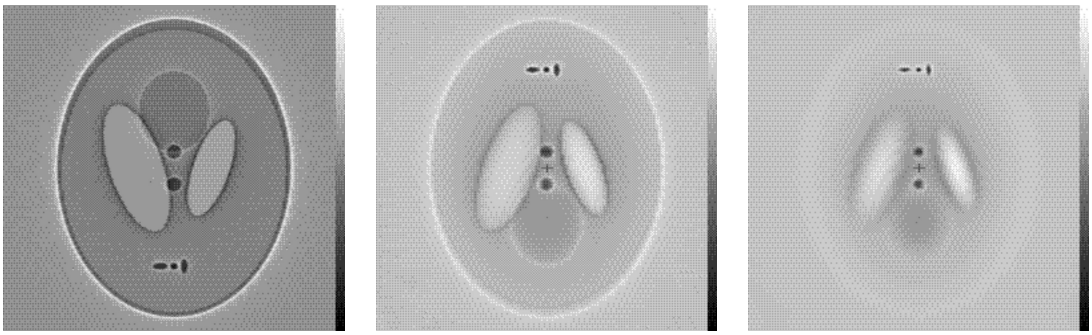

a) $\lambda = 0.5$ b) $\lambda = 1$ c) $\lambda = 2$

Fig. 7.
An application of the Vainberg operator to the Radon transform.

Figure 8 presents the results of a single application of the gradient module operator to the image of back-projection operator applied to the Radon transform of the potential 2 with different degree of smoothness.

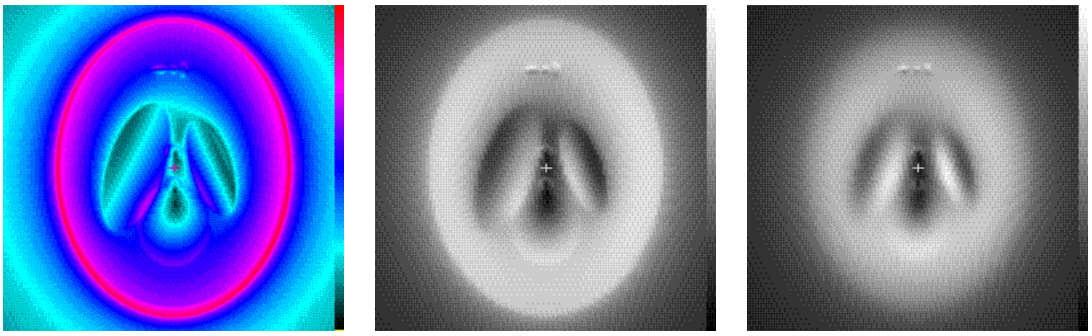

a) $\lambda = 0.5$ b) $\lambda = 1$ c) $\lambda = 2$

Fig. 8.
Results of a single application of GMO to BP.

Figure 9 presents the results of double application of the gradient module operator to the image of back-projection operator applied to the Radon transform of the potential 2 with different degree of smoothness.

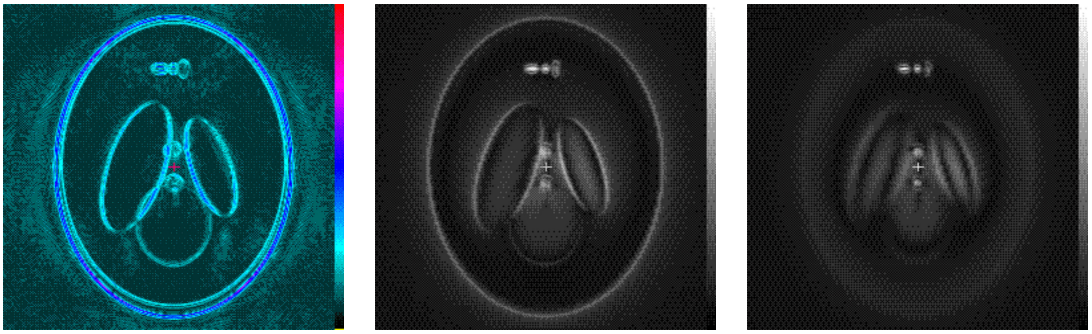

a) $\lambda = 0.5$ b) $\lambda = 1$ c) $\lambda = 2$

Fig. 9.
Results of a double application of GMO to BP.

Figures 10, 11 present "the parabolic Shepp-Logan phantom", named as "the potential 3" (Pot3), with $\lambda = 0.5$, $\lambda = 1$, which is a modification of "the potential 2". Figure 10 demonstrates results of a double application of the Vainberg operator to the image of the Radon transform of the potential 3.

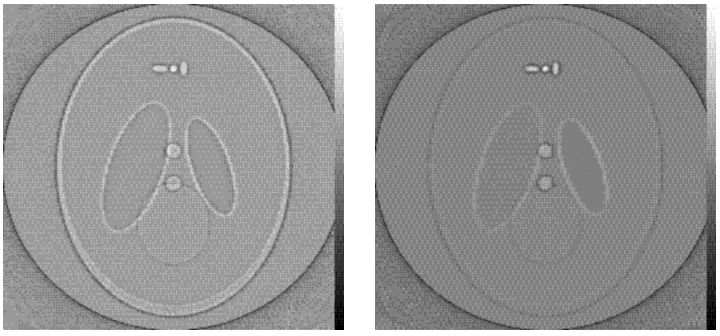

a) $\lambda = 0.5$ b) $\lambda = 1$

Fig. 10.
Double application of the Vainberg operator to the Radon transform of the Pot3.

Figure 11 presents results of a double and a triple application of the gradient module operator to the back-projection operator.

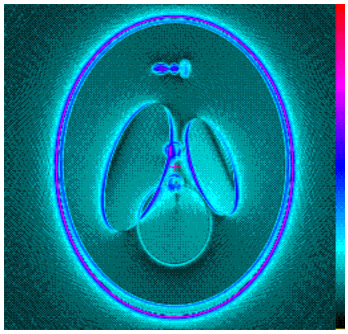

a) double GMO, $\lambda = 0.5$

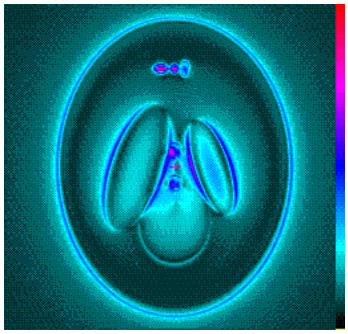

b) double GMO, $\lambda = 1$

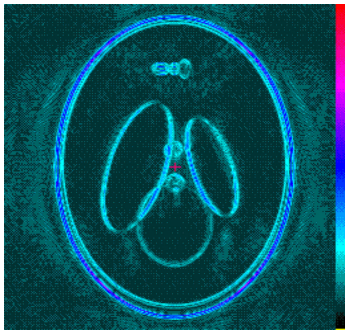

c) triple GMO, $\lambda = 0.5$

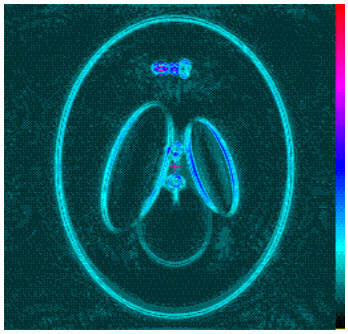

d) triple GMO, $\lambda = 1$

Fig. 11.
Results of double and triple application of the gradient module operator to the back-projection operator.

Test 3.3. A dependence of a quality of reconstruction of function and its first derivatives breaks from applied back-projection operators. The purpose of the third test is a visualization of singular support of the discontinuous function (Figure 12 a)

$$\varphi(x,y) = \begin{cases} 0.2, & \text{if } (x-0.3)^2 + y^2 < 0.04, \\ 0, & \text{otherwise,} \end{cases} \tag{22}$$

and the continuous function with discontinuous first derivatives (Figure 13 a)

$$\varphi(x,y) = \begin{cases} 0.1, & \text{if } (x-0.3)^2 + y^2 < 0.01, \\ 0.2 - \sqrt{(x-0.3)^2 + y^2}, & \text{if } 0.01 \leqslant (x-0.3)^2 + y^2 < 0.04, \\ 0, & \text{otherwise.} \end{cases} \tag{23}$$

We use the inner differentiation module operator as an operator of breaks indicator. Procedure of visualization of a singular support performed by two ways: with usage of the back-projection operator of the Radon transform (Figure 12 b and Figure 13 b); with usage of the back-projection operator of the longitudinal ray transform of the symmetric 2-tensor field (Figure 12 c and Figure 13 c).

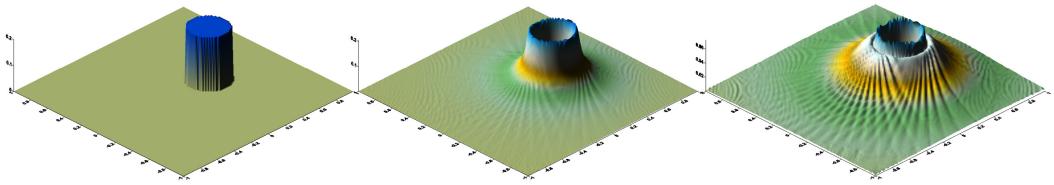

a) φ b) $|\nabla(\mathcal{R}^{\#}(\mathcal{R}\varphi))|$ c) $|\nabla(\mathcal{P}^{\#}_{2tf}(\mathcal{R}\varphi))|$

Fig. 12.
A function (22) (a); visualizations of its singular support by BP of the Radon transform (b); BP of the longitudinal ray transform of the symmetric 2-tensor field (c).

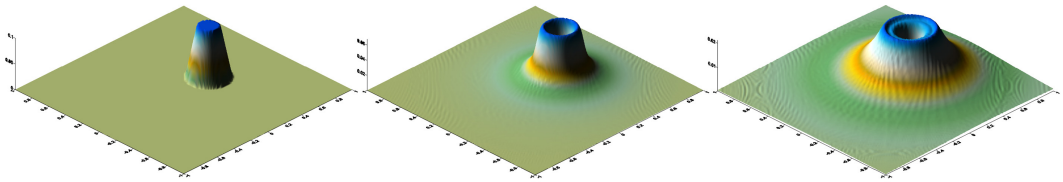

a) φ b) $|\nabla(\mathcal{R}^{\#}(\mathcal{R}\varphi))|$ c) $|\nabla(\mathcal{P}^{\#}_{2tf}(\mathcal{R}\varphi))|$

Fig. 13.
A function (23) (a); visualizations of its singular support by BP of the Radon transform (b); BP-operator of the longitudinal ray transform of the symmetric 2-tensor field (c).

We conclude from the figures, it is better to use an operator $|\nabla(\mathcal{R}^{\#}(\mathcal{R}\varphi))|$ for visualization of a singular support of a discontinuous field. Whereas for a function with discontinuous first derivatives an application of the operator $|\nabla(\mathcal{P}^{\#}_{2tf}(\mathcal{R}\varphi))|$ leads to the best results.

Test 3.4. A dependence of quality of reconstruction of a singular support of a small inclusion from its smoothness. The purpose of the fourth test is a visualization of singular support of the discontinuous scalar field with discontinuous inclusion (Figure 14 a)

$$\varphi(x,y) = \begin{cases} 1.2, & \text{if } x^2+y^2 < 0.25, \\ 1, & \text{if } 0.25 \leqslant x^2+y^2 < 1, \\ 0, & \text{otherwise,} \end{cases} \tag{24}$$

and the discontinuous scalar field with continuous inclusion (Figure 15 a)

$$\varphi(x,y) = \begin{cases} 1.2, & \text{if } x^2+y^2 < 0.04, \\ 4/3 - 2/3\sqrt{x^2+y^2}, & \text{if } 0.04 \leqslant x^2+y^2 < 0.25, \\ 1, & \text{if } 0.25 \leqslant x^2+y^2 < 1, \\ 0, & \text{otherwise.} \end{cases} \tag{25}$$

We use the gradient module operator, which is applied to the back-projection operator of the Radon transform, as an operator of breaks indicator. The breaks on the border of the unit circle gives a big splash, therefore the visualizations of the singular support are presented in a circle of radius 0.8.

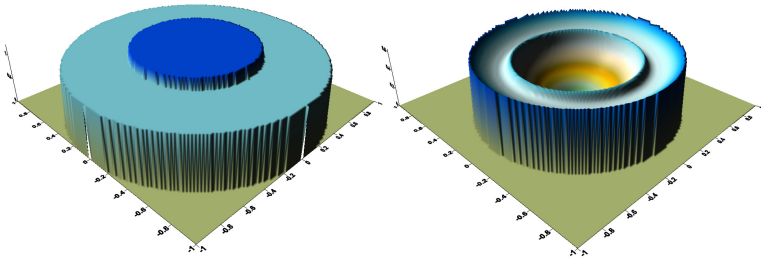

a) φ b) $|\nabla(\mathcal{R}^{\#}(\mathcal{R}\varphi))|$

Fig. 14.
The function (24) (a); visualizations of its singular support by BP-operator of the Radon transform (b).

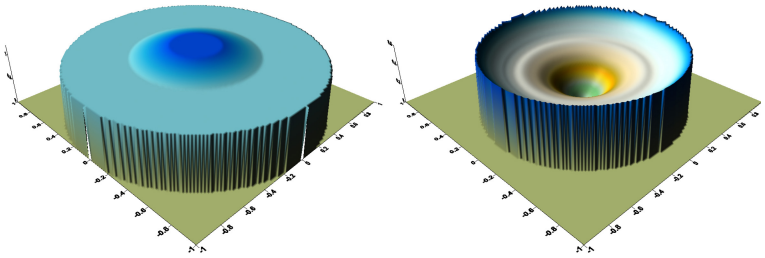

a) φ b) $|\nabla(\mathcal{R}^{\#}(\mathcal{R}\varphi))|$

Fig. 15.
The function (25) (a); visualizations of its singular support by BP-operator of the Radon transform (b).

The figures show that it is not enough to use a single application of the gradient module operator for visualization of a singular support of continuous inclusion (unlike discontinuous inclusion).

3.3 An action of the indicators of breaks on the Radon transform of a function with discontinuous derivatives

Test 3.5. A dependence of quality of reconstruction of derivatives breaks from the indicators of derivatives breaks. The purpose of the fifth test is a visualization of singular support of the continuous scalar field

$$\varphi(x,y) = h - \frac{h}{R}\sqrt{x^2+y^2}, \quad x^2+y^2 < R^2, \tag{26}$$

($h > 0$, $R > 0$ — parameters) with discontinuous first derivatives at the origin and on the boundary, i.e. $\partial D_0 = \partial D \cup \{(0,0)\}$. The initial data are values of the Radon transform, which can be easily calculated,

$$\big(\mathcal{R}\varphi\big)(\xi,s) = h\sqrt{R^2-s^2} - \frac{hs^2}{2R}\ln\frac{R+\sqrt{R^2-s^2}}{R-\sqrt{R^2-s^2}}. \tag{27}$$

Procedure of visualization of a singular support performed in three ways. At first, we use the the Vainberg operator (Fig. 16 c). Secondly, the operator $|\nabla^2(\cdot)|$ (Fig. 16 d),

and thirdly the operator $\operatorname{div}\nabla(\cdot)$ (Fig. 16 e), applied to the back-projection operator of the Radon transform of potential (27). Note that all three approaches give good result of visualization of derivatives breaks on the boundary ∂D, while the singularity at the origin are not determined by the Vainberg operator.

A reconstruction of a set of break points of a vector field can be carried out, in particular, by the following ways. Two ways at the first phase deal with calculation of the components μ_1, μ_2 using the formulas (9). Further (the first variant) $Q_1(x,y) = \nabla\mu_1(x,y)$, $Q_2(x,y) = \nabla\mu_2(x,y)$ and function $Q(x,y) = \sqrt{|Q_1|^2 + |Q_2|^2}$ is calculated. In the second variant $|\operatorname{div}\mu|$ is calculated.

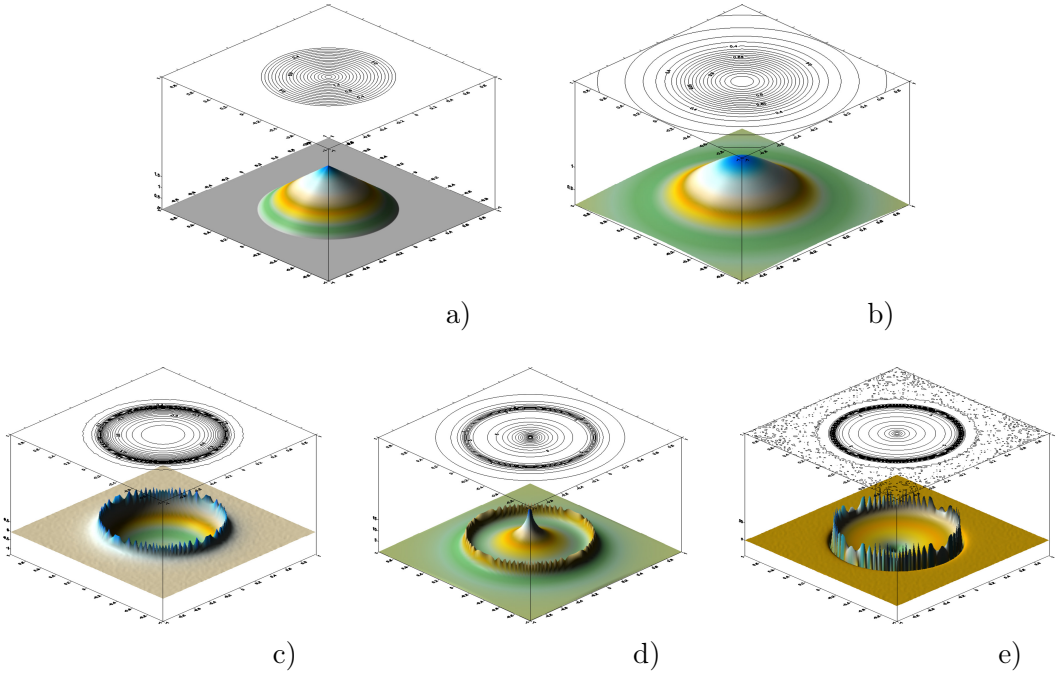

Fig. 16.
Potential (26) (a); BP-operator of (27) (b); visualization of the derivatives breaks: by the Vainberg operator (c); by the operator $|\nabla^2(\cdot)|$ (d); by the operator $\operatorname{div}\nabla(\cdot)$ (e).

Numerical experiments have shown good results of visualization of singular support of functions and vector fields. The gradient module operator, in general, proved to be more flexible instrument than the Vainberg operator. The last can not distinguish between breaks of function and breaks of its first derivatives. Application of the double differentiation (no matter by what operator) in some tests led to the appearance of the δ-function on lines of breaks, thus to a stronger singularity. However, the implementation of the described approaches has allowed to determine, visually, and this type of singularities.

4 A reconstruction of singular support of functions and vector fields

Discrete values of the images of the Radon transform of functions and discrete values of the images of the longitudinal and transverse ray transforms of vector fields

are the initial data for the reconstruction of the singular support of these fields. All other operators are the mathematical tools for solving the problem of reconstruction of geometric objects with not empty singular support. The first stage of the problem solving is a visualization of discontinuities or a singular support. In numerical tests a discrete grid of a size 256×128 for α, s is used. The number of rays for calculation of the back-projection operator is $N_\gamma = 256$. Figures of test fields and results of visualization of singular supports are given in the domain $[-1,1]^2$.

4.1 A reconstruction of breaks of the second derivatives of a function

Test 4.1. We consider the function with discontinuous second derivatives at the boundary. We name it as "parabolic hyperboloid × paraboloid squared" (Pot6),

$$\phi(x,y) = \begin{cases} xy\left(R^2-x^2-y^2\right)^2, & x^2+y^2<R^2 \\ 0, & x^2+y^2\geq R^2 \end{cases}. \tag{28}$$

This potential has the following Radon transform,

$$\begin{aligned}(\mathcal{R}\varphi)(\alpha,s) &= \int\limits_{-\sqrt{R^2-s^2}}^{\sqrt{R^2-s^2}} (s\cos\alpha - t\sin\alpha)\,(s\sin\alpha + t\cos\alpha)\left(R^2-s^2-t^2\right)^2 dt \\ &= -\frac{16}{105}\left(\sqrt{R^2-s^2}\right)^5\left(R^2-8s^2\right)\cos\alpha\sin\alpha.\end{aligned} \tag{29}$$

The partial derivative of the Radon transform with respect to s is equal to

$$\frac{\partial(\mathcal{R}\phi)(\alpha,s)}{\partial s} = \frac{16}{15}s\left(\sqrt{R^2-s^2}\right)^3\left(3R^2-8s^2\right)\cos\alpha\sin\alpha \tag{30}$$

The second partial derivative of the Radon transform (29) with respect to s is equal to

$$\frac{\partial^2(\mathcal{R}\phi)(\alpha,s)}{\partial s^2} = \frac{16}{5}\sqrt{R^2-s^2}\left(R^4-12s^2R^2+16s^4\right)\cos\alpha\sin\alpha$$

For visualization of breaks of the second derivatives of the function one has to use a triple differentiation which can be carried out either before or after application of the back-projection operator. Therefore many operators of breaks indicator arise for solving this problem. Operators of differentiation of the Radon transform with respect to s and α can be used, as well as all differential operators of vector analysis. They can be applied after the application of the back-projection operators. For example we may use the operators of gradient, curl and divergence.

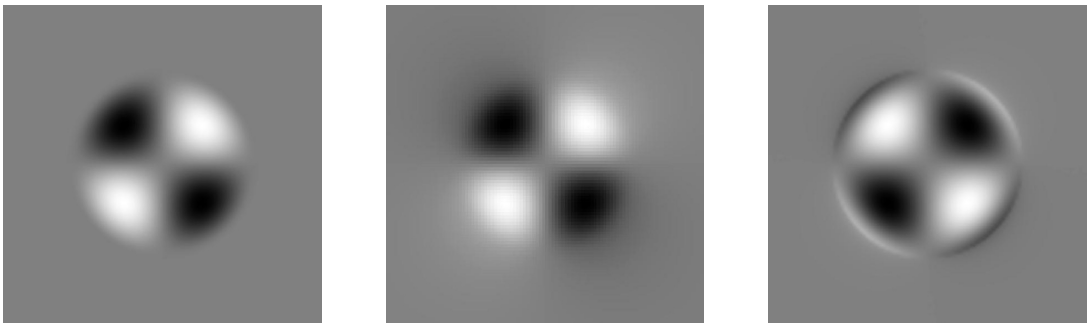

a) b) c)

Fig. 17.
The function Pot6 (a); application of the back-projection operator (b); application of the Vainberg operator (c).

The figure shows that it is not enough to use a double differentiation (the Vainberg operator) for visualization of a discontinuities of the second derivative of the scalar field.

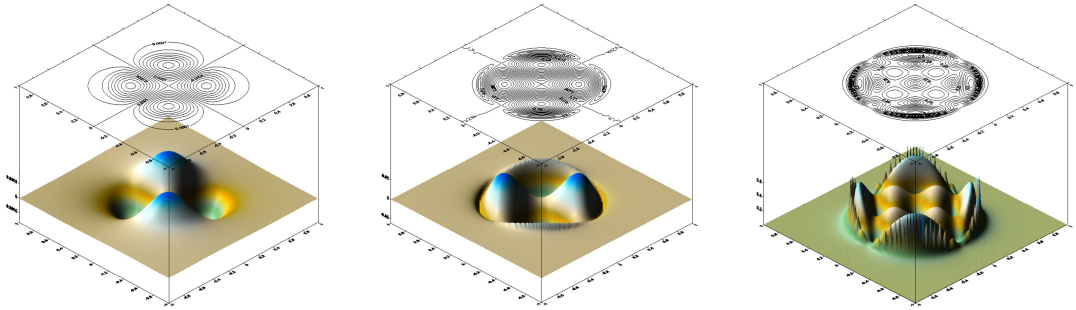

a) b) c)

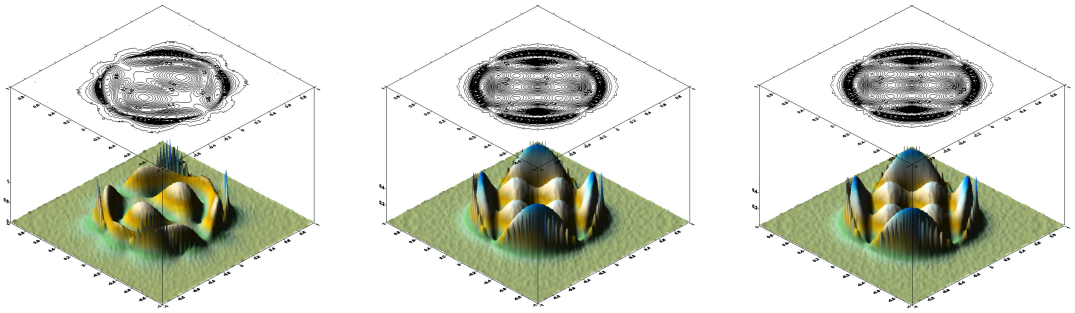

d) e) f)

Fig. 18.
The back-projection operator for the Pot6 (a); Vainberg operator (b); application of actions: the Vainberg operator, the operator $|\nabla(\cdot)|$ to the Radon transform of Pot6 (c); the operator $|\nabla^3(\cdot)|$ (d); the operators: ∇, div and $|\nabla(\cdot)|$ to the back-projection operator (e); the operator $|\mathrm{div}(\nabla(|\mathrm{rot}(\cdot)|))|$ (f).

We use four operators of breaks indicator. The figures show that it is not possible to single out any one indicator having a distinct advantage.

4.2 An action of the operators of breaks indicator to the ray transform of a vector field

Test 4.2. A dependence of quality of reconstruction of a vector field from the noise level. The solenoidal vector field is generated by the potential (in polar coordinates)

$$\varphi(x,y) = \begin{cases} r^2, & \text{if } |x| \le 1/4 \text{ and } |y| \le 1/4 \\ 4\pi - \phi, & \text{if } r \le \phi \text{ and } |x| > 1/4 \text{ and } |y| > 1/4 \\ 2\pi - \phi, & \text{if } \phi < r \le \phi + 2\pi \text{ and } |x| > 1/4 \text{ and } |y| > 1/4 \\ 0, & \text{otherwise} \end{cases}$$

and is defined by the relations $v_1 = \partial\varphi/\partial y$, $v_2 = -\partial\varphi/\partial x$. Figure 19 presents the potential and components of this field. Figure 20 demonstrates visualizations of discontinuities of the solenoidal vector field. An evenly distributed error with various levels is added to the initial data, i.e. in the longitudinal ray transform. We use the following noise levels: 0% (without noise), 5%, 10% and 20%. Figure 20 presents the result of application of the gradient module operator, i. e. $\varphi \to \nabla\varphi \to |\nabla\varphi|$, to an image of the back-projection operator, i. e. to a vector field (μ_1, μ_2).

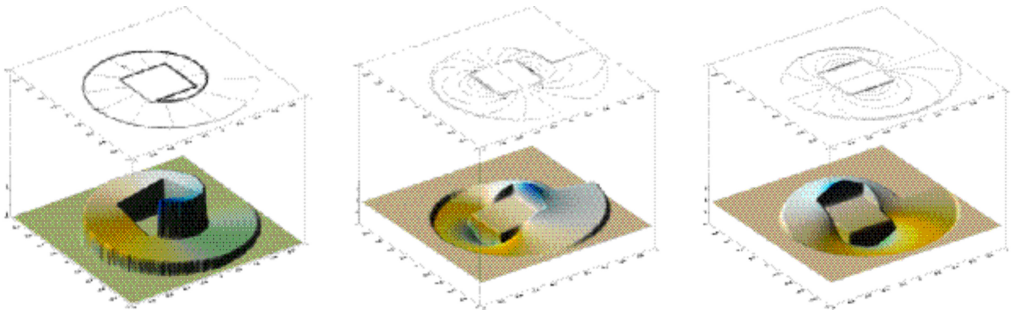

a) Potential VF b) Component 1 VF c) Component 2 VF

Fig. 19.
The potential and components of the solenoidal vector field.

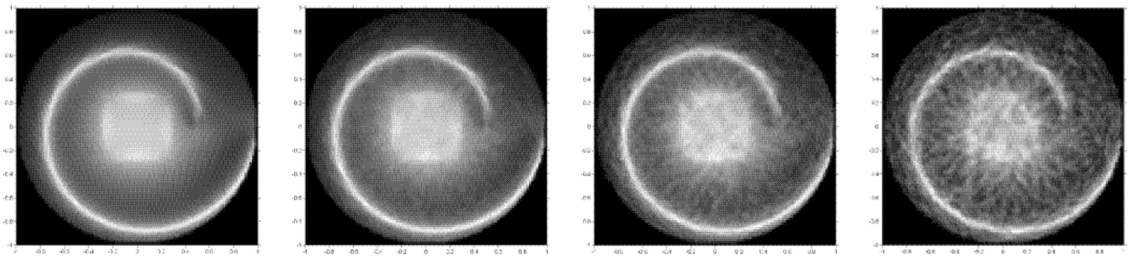

a) noise level 0% b) noise level 5% c) noise level 10% d) noise level 20%

Fig. 20.
Visualizations of breaks of the solenoidal VF. A uniformly distributed error with various levels is added in the initial data.

The figure 20 show that even a very large noise level in 20% allows us to identify the structure of the set of break points of the vector field.

4.3 An action of the operators of breaks indicator to the ray transform of a vector field with nonempty singular support

Test 4.3. Reconstruction of a set of break points of vector fields. Discontinuous solenoidal and potential vector fields are generated by the potential $\varphi(x,y) = h - h\sqrt{x^2+y^2}/R$ if $x^2+y^2 < R^2$ and $\varphi(x,y) = 0$ if $x^2+y^2 \geq R^2$. We used this potential above in Test 2.2.

The solenoidal vector field is defined by the formula

$$v = (v_1, v_2) = \begin{cases} \left(\dfrac{h}{R}\dfrac{y}{\sqrt{x^2+y^2}}, -\dfrac{h}{R}\dfrac{x}{\sqrt{x^2+y^2}}\right), & x^2+y^2 < R^2 \\ (0,0), & x^2+y^2 \geq R^2 \end{cases}, \tag{31}$$

and the potential vector field is defined by the formula

$$u = (u_1, u_2) = \begin{cases} \left(-\dfrac{h}{R}\dfrac{x}{\sqrt{x^2+y^2}}, -\dfrac{h}{R}\dfrac{y}{\sqrt{x^2+y^2}}\right), & x^2+y^2 < R^2 \\ (0,0), & x^2+y^2 \geq R^2 \end{cases}. \tag{32}$$

The transverse ray transform of the potential vector field (32) is calculated as follows

$$(\mathcal{R}v)(\theta, s) = -\frac{h}{R} s \ln \frac{R+\sqrt{R^2-s^2}}{R-\sqrt{R^2-s^2}}.$$

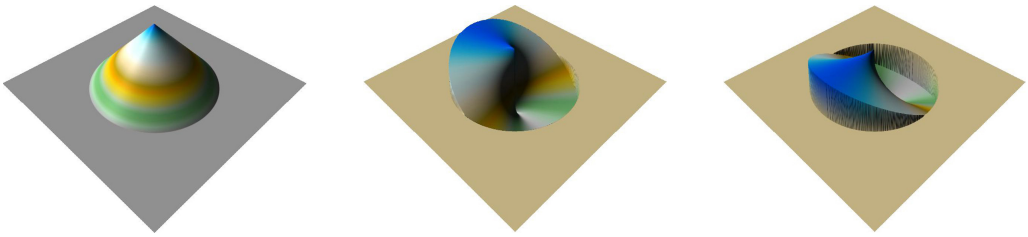

a) b) c)

Fig. 21.
The solenoidal VF (31). The potential ϕ of vector field (a); 1-st component of the field (b); 2-nd component of the field (c).

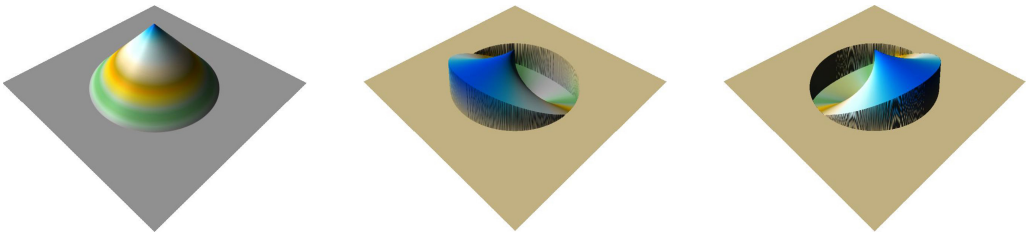

a) b) c)

Fig. 22.
The potential VF (32). The potential of VF 2 (a); 1-st component of the field (b); 2-nd component of the field (c).

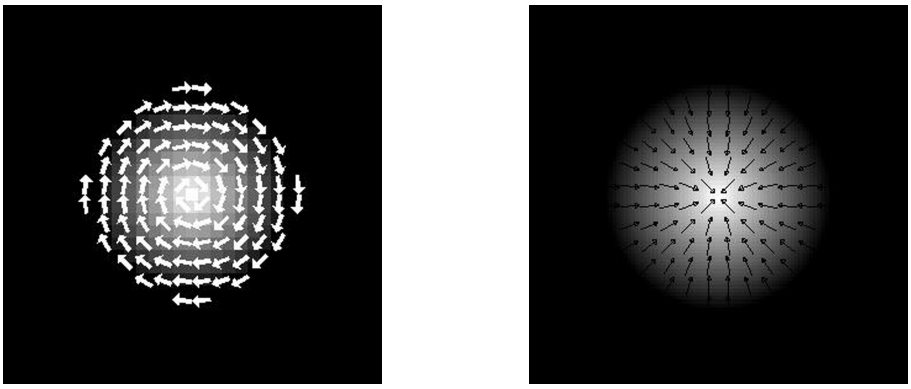

a) b)

Fig. 23.
Solenoidal VF (31) (a); potential VF (32) (b).

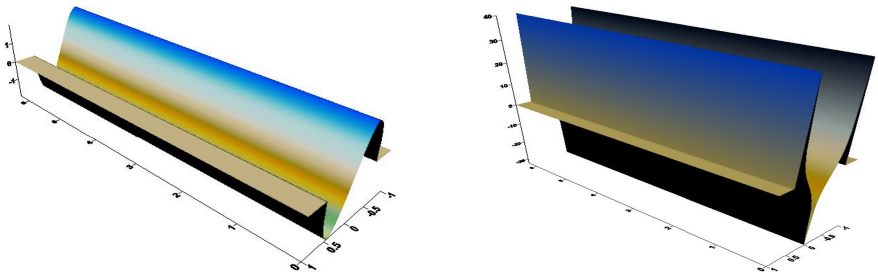

a) b)

Fig. 24.
The longitudinal (transverse) ray transform of the solenoidal (potential) VF (31) ((32)) (a); its derivative with respect to s (b).

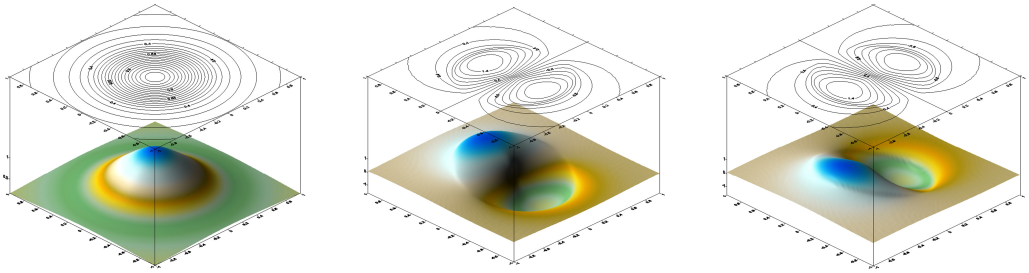

a) b) c)

Fig. 25.
Application of the back-projection operators: to the Radon transform of the potential (a); to the transverse ray transform of the potential VF (32), 1-st component λ_1 (b); 2-nd component λ_2 (c).

We recall that the components λ_1, λ_2 of the potential field (10) are produced by the action of the back-projection operator to the transverse ray transform of the field (32) by the formula (11). Besides that the longitudinal ray transform of solenoidal vector field and the transverse ray transform of potential vector field coincide if they are generated by the same potential. Therefore, the images on the Figure 25 (b) and (c) are at the same time also the result of application of the back-projection operator to the longitudinal ray transform of the solenoidal vector field (31).

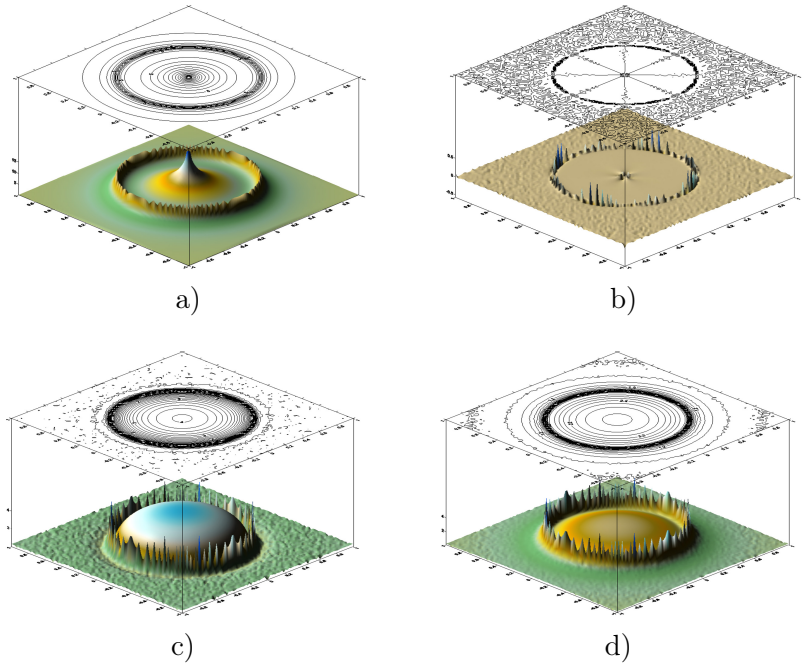

Fig. 26.
Reconstruction of breaks of VF (32). Application of the operator $|\nabla^{\perp}(\cdot)|$ to the vector field λ (a); application of the operator $\mathrm{div}^{\perp}$ to λ (b); application of the back-projection operator (with respect to the function) after application of differentiation with respect to s to the ray transform of field (32) (c); application of the back-projection operator (with respect to the 2-tensor field) after application of differentiation with respect to s to the ray transform of field (32) (d).

A procedure of visualization of breaks of a field can be performed, in particular, by the following four ways. In the first two at the first stage we calculate the components λ_1, λ_2 of a vector field obtained by application of the back-projection operator to the transverse ray transform of original field. Further (the first variant) we calculate $Q_1(x,y) = \nabla^{\perp}\lambda_1(x,y)$, $Q_2(x,y) = \nabla^{\perp}\lambda_2(x,y)$, and then the function $Q(x,y) = \sqrt{|Q_1|^2 + |Q_2|^2}$. Second variant consists in calculation of $|\mathrm{div}^{\perp}\mu|$. The third and fourth ways contain the first stage in differentiation with respect to s. Further the image of the back-projection operator with respect to the function (the third variant), and the image of the back-projection operator with respect to the 2-tensor field (the fourth variant) are calculated.

In the test the initial data for the solution of the problem are the transverse ray transform of the potential vector field with the potential, which was used in test 2.2 for a construction of the solenoidal vector field. Comparison of Figures 4 and 26 allows us to conclude that results of visualizations of the set of break points of two fields are the same, as would be expected.

Test 4.4. Reconstruction of breaks of first derivatives of a vector field. A vector field 6 is generated by the potential 6 (Pot6) with discontinuous 1-st derivatives on the boundary. The potential

$$\phi(x,y) = \begin{cases} xy\left(R^2 - x^2 - y^2\right)^2, & x^2 + y^2 < R^2 \\ 0, & x^2 + y^2 \geq R^2 \end{cases}$$

generates the solenoidal vector field

$$v = (v_1, v_2) = \begin{cases} (R^2 - x^2 - y^2)\Big(- x(R^2 - x^2 - 5y^2)\,, \\ \qquad\qquad y(R^2 - 5x^2 - y^2)\Big), & x^2 + y^2 < R^2 \\ (0,0), & x^2 + y^2 \geq R^2 \end{cases},$$

and the potential vector field

$$u = (u_1, u_2) = \begin{cases} (R^2 - x^2 - y^2)\Big(y(R^2 - 5x^2 - y^2)\,, \\ \qquad\qquad x(R^2 - x^2 - 5y^2)\Big), & x^2 + y^2 < R^2 \\ (0,0), & x^2 + y^2 \geq R^2 \end{cases}.$$

The potential of the fields is continuous function in $\mathbb{R}^2$, so the longitudinal (transverse) ray transform of the solenoidal (potential) vector field 6 coincides with the first partial derivative with respect to s of the Radon transform (30) of the potential (28),

$$(\mathcal{R}v)(\theta, s) = \frac{16}{15} s \left(3R^2 - 8s^2\right) \left(R^2 - s^2\right)^{3/2} \theta^1 \theta^2$$

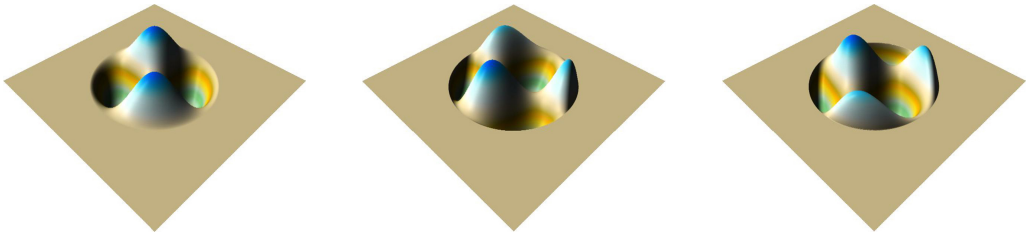

a) b) c)

Fig. 27.
The solenoidal VF 6. The potential ϕ of VF 6 (a); 1-st component $-\partial\phi/\partial y$ of the field (b); 2-nd component $\partial\phi/\partial x$ of the field (c).

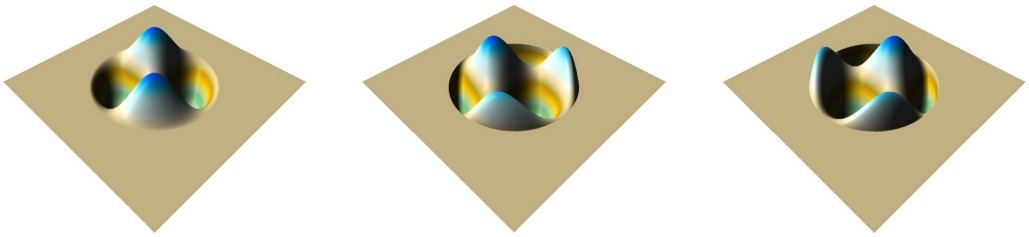

a) b) c)

Fig. 28.
The potential VF generated by the potential 6. The potential ϕ of VF 6 (a); 1-st component $\partial\phi/\partial x$ of the field (b); 2-nd component $\partial\phi/\partial y$ of the field (c).

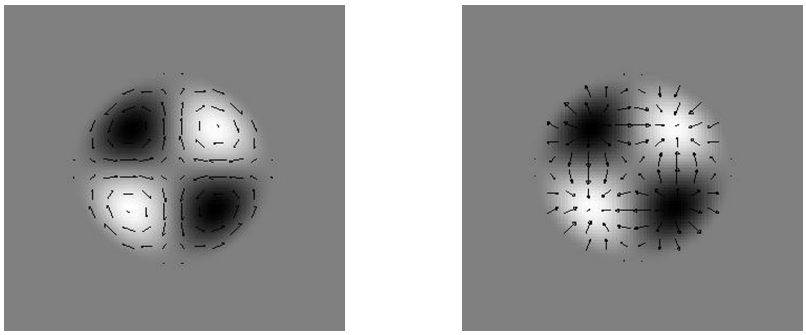

a) b)

Fig. 29.
The solenoidal VF (a) and the potential VF (b) generated by the Pot. 6.

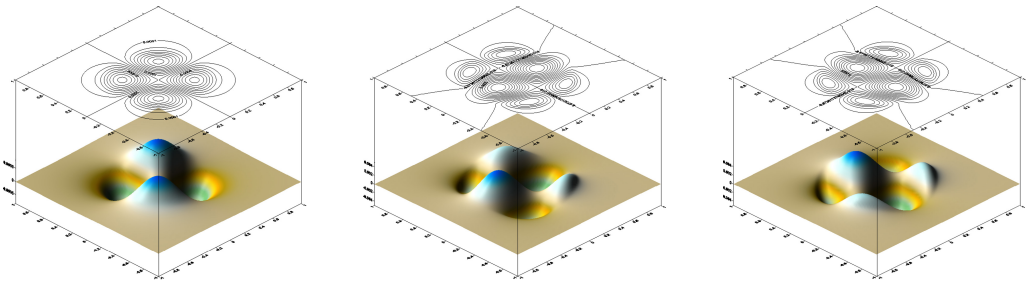

a) b) c)

Fig. 30.
Application of the back-projection operators: to the Radon transform of potential 6 (a); to the longitudinal ray transform of solenoidal VF 6, 1-st component μ_1 (b); 2-nd component μ_2 (c).

Figures 31–33 demonstrate different reconstructions of the set of break points of the first derivatives of solenoidal vector field generated by the potential 6. At the first figure the operator of the angular momentum of the 1-st order, coinciding with the back-projection operator with respect to vector field, is applied to the known longitudinal ray transform. The result is a vector field (μ_1, μ_2). Then we apply the gradient operator to (μ_1, μ_2) two times and calculate module of 3-tensor field, Fig. 31 (a); we apply the gradient operator, the divergence operator, and calculate the module of resulting vector field, Fig. 31 (b); finally, we apply the divergence operator, the gradient operator, and calculate module of resulting vector field, Fig. 31 (c).

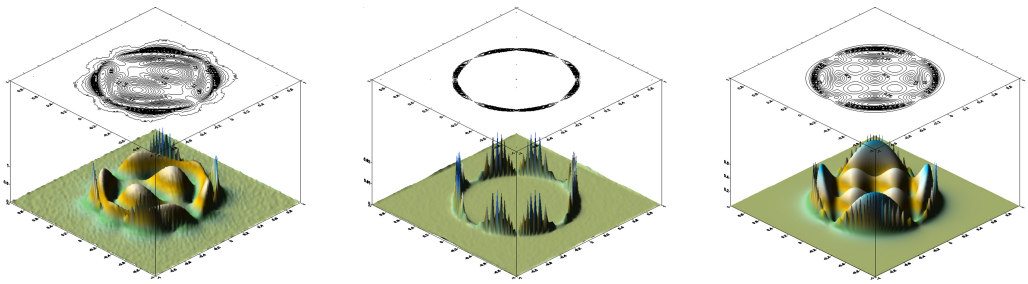

a) b) c)

Fig. 31.
Reconstruction of breaks of the first derivatives of VF 6. After application of the back-projection operator we calculate the module of results of: the double gradient operator (a); the gradient and divergence operators (b); the divergence and gradient operators (c).

Figure 32 represents the results obtained with usage of other procedures. Namely, primarily the operator of differentiation over s is applied to the ray transform. The result is the longitudinal ray transform of symmetric solenoidal 2-tensor field generated by the potential 6. The resulting function is even, as the Radon transform of the potential 6. Therefore, it is possible to apply the operators of angular moments of even orders to this function (the operators of angular moments of odd orders give identical 0, as already mentioned). Figure 32 (a) demonstrates the result of application of sequence of operators: the differentiation operator with respect to s, the operator of angular moments of the zero order (as to the Radon transform of the scalar field), the gradient operator, the module of resulting vector field. Figures 32 (b, c) present results of application of the operator of angular moments of the second order, coinciding with the back-projection operator of the longitudinal ray transform of symmetric solenoidal 2-tensor field, to the result of application of the differentiation operator with respect to s. Further we apply the divergence operator and calculate module of the resulting vector field (Fig. 32 (b)); we apply the gradient operator and calculate module of the resulting 3-tensor field (Fig. 32 (c)).

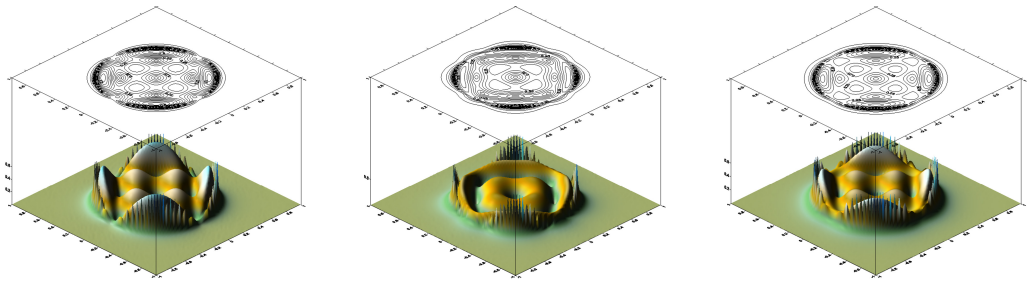

a) b) c)

Fig. 32.

Reconstruction of breaks of the first derivatives of VF 6. Application of operators: the differentiation operator with respect to s, the back-projection operator with respect to scalar field, the gradient operator, the module of resulting VF (a); the differentiation operator with respect to s, the back-projection operator with respect to symmetric 2-tensor field (b, c), then the calculate of divergence and its module (b); gradient and its module(c).

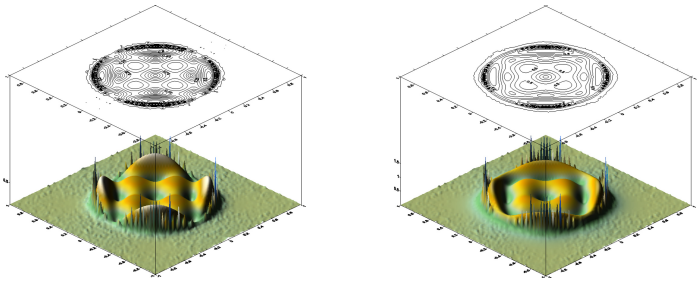

a) b)

Fig. 33.

Reconstruction of breaks of the first derivatives of VF 6. After application of double differentiation operator with respect to s to the ray transform we apply the back-projection operator with respect to VF and calculate module of the result (a); we apply the back projection operator with respect to symmetric 3-tensor field and calculate module of the result (b).

Figure 33 presents results of application (in the first stage) of the double differentiation with respect to s to the ray transform. The result is the longitudinal ray transform of symmetric solenoidal 3-tensor field generated by the potential 6. The resulting function is odd, as and the longitudinal ray transform of solenoidal vector field 6. Therefore it is possible to apply the operators of angular moments of odd orders to this function (in this case the operators of angular moments of even orders give identical 0 as a result). Figure 33 (a) demonstrates the result of application of the following operators: the double differentiation with respect to s; the operators of angular moments of the first order; the module of resulting vector field. Figure 33 (b) presents the result of application of the following operators: the double differentiation with respect to s; the operators of angular moments of the third order, which coincide with the back-projection operator of the longitudinal ray transform of symmetric solenoidal 3-tensor field; the module of resulting 3-tensor field.

4 Conclusion

Stated above settings and features of the problems of scalar, vector and tensor tomography at applications to the geometrical objects with breaks and geometrical objects with non-empty singular support lead to certain outlines and conclusions. Principles of formations for the procedures of initial data obtaining are based on quite different physical effects. Often they are very differ from the lying at the base of transmission tomography the phenomenon of attenuation of a signal intensity at passage throw the continuous medium. We recall that at a base of measuring in the most known problems of vector and tensor tomography lay very different physical concepts. They are difference between flight-of-times of direct and inverse signals in investigations of liquid and gas currents, the Doppler effect, schlieren-effect, a phenomenon of electromagnetic and elastic waves polarization, etc.

The questions arise naturally weather the method and algorithms developed for the problems of computer (scalar) tomography can be applied for the problems of vector and tensor tomography? Especially since we investigate the objects with discontinuous properties? Either they need in constructions of new mathematical tools which differs very much from developed in framework of "tomography of functions"? Do they need in special mathematics, methods and algorithms for every problem of vector or tensor tomography based on different physical effects? Just now we may answer the first two questions positively, but for the other questions the answers are negative at general. The settings of 2D-tomography problems of vector and tensor fields confirm these answers obviously. The variety of physical phenomena lying at the measurements of passed through the objects physical fields in corresponding mathematical models are leveling, but the mathematical models of data registrations are reduced to few types of ray transforms. Besides, very different physical effects can be led to the same type of ray transform. Raspingly speaking the problem of reconstruction of a tensor field (and with non-empty singular support) by its known ray transforms can be reduced to the problem of reconstruction of its components considered as functions by their Radon transforms. Hence the vast majority of the approaches and algorithms developed for the problems of function reconstruction can be applied and to the problems of vector

and tensor tomography, if we restrict ourselves by investigations of the media without refraction.

In the article necessary denotations, definitions, primary information on vector and tensor fields as well as on main tomographic operators, such as the Radon and ray transforms, the operator of back-projection and angular moment, are presented. We formulate certain properties of the operators and pay attention to the inversion formulaes. In particular we present the inversion formulaes giving the potentials of vector fields.

A main goal of the article consists in confirmation and description of generalization of the problem of function breaks reconstruction by the Radon transform. We suggest to reconstruct the singular support of scalar, vector and tensor fields by their known Radon or ray transforms. We describe the methods of the operators of indicators of inhomogeneity and breaks construction with usage of the differential operators of tensor analysis, the back-projection and angular moment operators. The differential operators d, $\mathrm{d}^{\perp}$, δ, $\delta^{\perp}$ are applied widely for mathematical modeling and numerical simulations.

In the article we summarize new approaches, methods and algorithms for the problems of breaks of discontinuous functions and vector fields solving, as well as for the problems of a singular support of tensor fields reconstruction. Tomographic information such as the values of the Radon transform and the longitudinal and transverse ray transforms are exploited as initial data for the problems. A number of numerical tests are provided, and their results are demonstrated. The results are satisfactory and show that our approaches and algorithms constructed on a base of proposed operators of indicators of breaks of functions and vector fields are working good with the numerous test examples.

References

[1] J. Radon, *Über die Bestimmung von Funktionen durch ihre Integrabwerte längs gewisser Mannigfaltigkeiten*, Berichte Sächsische Akademie der Wissenschaften, Vol. 69 (1917), 262–277.

[2] P. Funk, *Über eine geometrische Anwendung der Abelschen Integralgleichung*, Math. Ann., Vol. 77 (1916), 129–135.

[3] M.M. Lavrent'ev, V.G. Romanov, S.P. Shishatskii, *Ill-possed problems of mathematical physics and analysis*, Translations of Mathematical Monographs, Vol. 64, American Mathematical Sosiety, Providence, 1986.

[4] I.M. Gelfand, M.I. Graev, N.Ya. Vilenkin, *Generalized functions. Vol. 5: Integral geometry and representation theory*, Translated from the Russian by Eugene Saletan, Academic Press, Boston, 1966.

[5] I.M. Gelfand, S.G. Gindikin, M.I. Graev, *Selected topics in integral geometry*, Translations of Mathematical Monographs, Vol. 220, American Mathematical Society, Providence, 2003.

[6] V.G. Romanov, *Inverse Problems of Mathematical Physics*, VNU Science Press, Utrecht, 1987.

[7] V.G. Romanov, S.I. Kabanikhin, *Inverse Problems for Maxwell's Equations*, VSP, Utrecht, 1994.

[8] V.R. Kireitov, *Inverse Problems of Photometry*, Novosibirsk, Computing Center of the USSR Acad. Sci., 1983 (in Russian).

[9] Yu.E. Anikonov, L.N. Pestov, *Formulas in linear and nonlinear problems of tomography*, Novosibirsk, Novosibirsk Univ. Press, 1990 (in Russian).

[10] V.A. Sharafutdinov, *Integral Geometry of Tensor Fields*, Utrecht: VSP, 1994.

[11] L.N. Pestov, *Well-Posedness Questions of the Ray Tomography Problems*, Novosibirsk, Siberian Science Press, 2003 (in Russian).

[12] S.I. Kabanikhin, *Inverse and Ill-Posed Problems. Theory and Applications*, De Gruyter, Germany, 2011.

[13] G. Nolet (Ed.), *Seissmic tomography: with applications in global seismology and exploration geophysics*, D. Reidel Publishing Company, Dordrecht, Holland, 1987.

[14] R.N. Bracewell, A.C. Riddle, *Inversion of fan-beam scans in radio astronomy*, The Astrophysical Journal, Vol. 150 (1967), 427–434.

[15] G.N. Ramachandran, A.N. Lakshminarayanan, *Three-dimensional reconstruction from radiographs and electron micrographs: application of convolutions instead of Fourier transforms*, Proc. Nat. Acad. Sci. US, Vol. 68 (1971), 2236–2240.

[16] L.A. Shepp, B.F. Logan, *The Fourier reconstruction of a head section*, IEEE Trans. Nucl. Sci., Vol. NS-21 (1974), 21–43.

[17] F. Natterer, *The Mathematics of Computerized Tomography*, Wiley, Chichester, 1986.

[18] R.N. Bracewell, *Image reconstruction in radio astronomy*, in: Herman G.T. (ed.), Image Reconstruction from Projections, Springer, 1979.

[19] R.A. Crowther, D.J. De Rosier, A. Klug, *The reconstruction of a three-dimensional structure from projections and its application to electron microscopy*, Proc. R. Soc. London Ser. A, Vol. 317 (1970), 319–340.

[20] R. Gordon, R. Bender, G.T. Herman, *Algebraic reconstruction techniques (ART) for three-dimensional electron microscopy and X-ray photography*, J. Theor. Biol., Vol. 29 (1970), 471–481.

[21] G.N. Hounsfield, *Computerized transverse axial scanning tomography: Part 1, description of the system*, Br. J. Radiol., Vol. 46 (1973), 1016–1022.

[22] I.M. Gelfand, A.B. Goncharov, *Reconstruction of a compactly supported function by its integrals over the lines intersecting a curve in the space*, Sov. Math. Dokl., Vol. 34 (1987), 373–376.

[23] D.S. Anikonov, A.E. Kovtanyuk, I.V. Prokhorov, *Transport Equation and Tomography*, VSP, Utrecht, The Netherland, 2002.

[24] E.I. Vainberg, I.A. Kazak, M.L. Faingoiz, *X-ray computerized back projection tomography with filtration by double differentiation. Procedure and information features*, Soviet J. Nondest. Test, No. 21 (1985), 106–113.

[25] A. Faridani, F. Keinert, F. Natterer, E.L. Ritman, K.T. Smith, *Local and global tomography*, Signal Process., IMA Vol. Math. Appl., Springer-Verlag, New York, Vol. 23 (1990), 241–255.

[26] A. Faridani, E.L. Ritman, K.T. Smith, *Local tomography*, SIAM J. Appl. Math., Vol. 52, 2 (1992), 459–484.

[27] A. Faridani, D.V. Finch, E.L. Ritman, K.T. Smith, *Local tomography II*, SIAM J. Appl. Math., Vol. 57, 4 (1997), 1095–1127.

[28] A.K. Louis, P. Maass, *Contour Reconstruction in 3-D X-Ray CT*, IEEE Trans. Med. Imag., Vol. 12, 4 (1993), 764–769.

[29] S.G. Mihlin, *Multidimensional singular integrals and integral equations*, Pergamon Press, New York, 1965

[30] D.S. Anikonov, *Use of the features of the solution of the transport equation in the X-ray tomography*, Reports of the Russian Academy of Sciences, Vol. 335, 6 (1994), 702–704 (in Russian).

[31] D.S. Anikonov, *A special problem of integral geometry*, Doklady Mathematics, Vol. 76 (2007), 483–485.

[32] V. Sharafutdinov, M. Skokan, G. Uhlmann, *Regularity of ghosts in tensor tomography*, J. Geom. Analysis, Vol. 15, 3 (2005), 499–542.

[33] E.Yu. Derevtsov, *Some approaches to a reconstruction of a singular support of scalar, vector and tensor fields by their known tomographic data*, Sib. Electron. Math. Izv., Vol. 5 (2008), 632–646 (in Russian).

[34] E.Yu. Derevtsov, V.V. Pickalov, *Reconstruction of vector fields and their singularities from ray transform*, Num. Anal. Appl., Vol. 4, 1 (2011), 21–35.

[35] A.P. Polyakova, I.E. Svetov, E.Yu. Derevtsov, M.A. Sultanov, *On the problem of the recovery and identification of the set of points of breaks of the geometrical objects by tomography data*, Joint issue "Computational Technologies", Vol. 20 (2015) and "The KazNU Journal: Mathematics, Mechanics and Computer Science Edition", No. 3(86) (2015), part I, 346–358 (in Russian).

[36] E.Yu. Derevtsov, S.V. Maltseva, I.E. Svetov, *Construction of the operators of indicator of breaks for tensor fields of small rank by their ray transforms*, Joint issue "Computational Technologies", Vol. 20 (2015) and "The KazNU Journal: Mathematics, Mechanics and Computer Science Edition", No. 3(86) (2015), part III, 231–243 (in Russian).

[37] E.Yu. Derevtsov, A.S. Kasymbekov, S.V. Maltseva, I.E. Svetov, M.A. Sultanov, *On reconstruction of discontinuous functions by tomographic data*, Abstracts of the Internation Conference "Differential Equations and Mathematical Modeling", June 22–27, 2015, Ulan–Ude — Lake Baikal, Russia, 97–98.

[38] N.E. Kochin *Vector Calculus and Fundamentals of Tensor Calculus*, Leningrad–Moskow, Gos. Tech.-Teor. Izd., 1934 (in Russian).

[39] H. Weyl, *The method of orthogonal projection in potential theory*, Duke Math. J., Vol. 7 (1940), 411–444.

[40] S.L. Sobolev, *On a new problem of mathematical physics*, Izv. Akad. Nauk SSSR, Ser. Mat., Vol. 18, 1 (1954), 3–50 (in Russian).

[41] E.Yu. Derevtsov, I.E. Svetov, *Tomography of tensor fields in the plane*, Eurasian J. Math. Comp. Applications, Vol. 3, 2 (2015), 24–68.

[42] I.S. Gradshtein, I.M. Ryzhik *Tables of integrals, series and products*, 4th edition, State publishing physical and mathematical literature, Moskow, 1963 (in Russian).

[43] S. Deans, *The Radon transform and some of its applications*, New York, Wiley, 1983.

Evgeny Yurievich Derevtsov,
Sobolev Institute of Mathematics SB RAS,
4, Akademika Koptyuga Prospect, Novosibirsk, Russia.
Novosibirsk State University,
2, Pirogova Street, Novosibirsk, Russia.
Email: dert@math.nsc.ru,
Svetlana Vasilievna Maltseva,
Sobolev Institute of Mathematics SB RAS,
4, Akademika Koptyuga Prospect, Novosibirsk, Russia.
Novosibirsk State University,
2, Pirogova Street, Novosibirsk, Russia.
Email: sv-maltseva@mail.ru,
Ivan Evgenyevich Svetov,
Sobolev Institute of Mathematics SB RAS,
4, Akademika Koptyuga Prospect, Novosibirsk, Russia.
Novosibirsk State University,
2, Pirogova Street, Novosibirsk, Russia.
Email: svetovie@math.nsc.ru,

Received 25.11.2015, Accepted 7.12.2015